

II. OPEN ISSUES FOR p - p COLLISIONS

We present a summary of issues introduced in Sec. I including p - p centrality in relation to a conjectured underlying event, manifestations of MB dijets in spectra and correlations and existence and interpretation of a NJ quadrupole component of p - p 2D angular correlations.

A. p - p centrality and the underlying event

Item (a) of Sec. I relates to interpretations of deep-inelastic scattering (DIS) data to indicate that low- x gluons are concentrated within a transverse region of the proton substantially smaller than its overall size. It is argued that a high- p_t dijet trigger may select more-central p - p collisions with greater soft-hadron production [1]. The soft (nonjet) multiplicity increase should be observed most clearly within a narrow azimuth *transverse region* (TR) centered at $\pi/2$ and thought to *exclude contributions from the triggered jets* centered at 0 and π .

Item (b) relates to measurements of charge multiplicity N_\perp within the TR vs trigger condition $p_{t, trig}$ and dN_\perp/dp_t spectra employed to characterize the UE [2, 3]. Substantial increase of N_\perp with higher $p_{t, trig}$ relative to a minimum-bias or non-single-diffractive (NSD) value is interpreted to reveal novel contributions to the UE, including *multiple parton interactions* (MPI) corresponding to a high rate of dijet production [14]. Monte Carlo p - p collision models such as PYTHIA [15] are tuned to accommodate such results [16].

In Ref. [12] items (a) and (b) were considered in the context of a two-component (soft+hard) model (TCM) of hadron production as manifested in yields and spectra. It was observed that imposing a p_t trigger condition on events does lead to selection for *hard events* (containing at least one dijet) but that the soft component of the selected events is not significantly different from a MB event sample, in contrast to expectations from Ref. [1] that increased dijet frequency should correspond to more-central p - p collisions and therefore to a larger soft component from low- x gluons. Since n_{ch} apparently determines dijet rates directly [4] it might also control p - p centrality, but Ref. [12] concluded that further p - p correlation measurements are required to explore that possibility. The present study responds with the n_{ch} dependence of MB dijet correlations and NJ quadrupole systematics that speak to the issue of p - p centrality and UE systematics.

B. Manifestations of minimum-bias dijets

Item (c) relates to the role of MB dijets in yields, spectra and various types of two-particle correlations. The contribution of MB dijets (minijets [17]) to SP p_t spectra was established in Refs. [4, 18, 19], and the contribution of minijets to 2D angular correlations was identified in Refs. [5, 6, 20, 21]. However, further effort is required

to establish a complete and self-consistent description of MB dijets in p - p and A - A yields, spectra and correlations.

In Ref. [20] item (c) was addressed with 2D model fits applied to angular correlations from Au-Au collisions at 62 and 200 GeV to isolate several correlation components, including structures attributed to MB dijets and a NJ quadrupole, with emphasis on the former in that study. The systematics of two components (soft + hard) are consistent with the TCM. The dijet (hard-component) trend on centrality exhibits a *sharp transition* near 50% fractional cross section below which Au-Au collisions appear to be simple linear superpositions of N - N binary collisions (transparency) and above which *quantitative* changes in the dijet component appear, but not in the NJ quadrupole component [7]. The MB dijet interpretation has been questioned variously, for more-central A - A collisions [22] or for all nuclear collisions [23].

We wish to confirm the role of MB dijets as such via a self-consistent description of Au-Au *and* p - p collisions based on QCD theory. Although a TCM for p - p yields and spectra vs n_{ch} has been established [4, 19] the systematics of MB dijet production in p - p collisions is incomplete. MB 2D angular correlations for p - p collisions have been decomposed into soft and hard components via a single p_t cut (at 0.5 GeV/c) [5], but a TCM for p - p angular correlations vs n_{ch} has not been available. In Ref. [21] Au-Au MB jet-related correlation structure vs centrality was related quantitatively to spectrum hard components (dijets) to establish a direct link of both data formats with pQCD predictions. In the present study we carry out a similar analysis of p - p vs n_{ch} trends.

We also extend the p - p TCM established on marginal y_t to the 2D (y_t, η) system to determine the distribution of minijets on the full SP momentum space. The extension to η may provide further evidence that a MB dijet interpretation of the inferred TCM hard component is *necessary* as a distinct element of hadron production.

C. Nonjet azimuth quadrupole

Item (d) relates to the possibility of a significant amplitude for a unique azimuth quadrupole in p - p collisions. (The NJ quadrupole should be distinguished from the quadrupole component of a *jet-related* 2D peak projected onto 1D azimuth.) Measurements of a NJ quadrupole component of angular correlations in Au-Au collisions (conventionally represented by parameter v_2) are found to be consistent with a simple universal trend on centrality and collision energy extrapolating to a nonzero value for N - N collisions [9]. The extrapolation is consistent with a QCD-theory prediction for v_2 in p - p collisions [24].

The p - p NJ quadrupole may be related to a same-side “ridge” reported in p - p collisions at 7 TeV (with special cuts on p_t and n_{ch} imposed) [11, 25]. It has been suggested that the p - p same-side ridge arises from the same mechanism proposed for A - A collisions based on collective motion (flows) coupled to initial-state collision ge-

ometry. Systematics of a possible NJ quadrupole in p - p collisions have thus emerged as an important new topic.

Reference [11] considered extrapolation of NJ quadrupole centrality systematics in 200 GeV Au-Au collisions to N - N collisions, and further extrapolation to LHC energies based on measured RHIC energy dependence. In that scenario the same-side ridge observed in LHC p - p collisions corresponds to one lobe of the NJ quadrupole. The other lobe is obscured by the presence of a dominant away-side (AS) 1D jet peak. Quantitative correspondence was observed in Ref. [11] suggesting that the NJ quadrupole may play a significant role in p - p collisions, but no direct p - p quadrupole measurements existed. This study offers a response to that issue.

Measurement of NJ quadrupole trends may shed light on the question of p - p centrality [item (a)] by analogy with A - A quadrupole systematics wherein the NJ quadrupole measured by a *per-particle* variable first increases rapidly with centrality and then falls sharply toward zero with decreasing A - A eccentricity, as described by a Glauber model based on the eikonal approximation. Since dijet production vs n_{ch} in p - p collisions suggests that the eikonal approximation is not valid for that system [26, 27] the NJ quadrupole trend could provide a critical test of the eikonal assumption for p - p collisions.

III. ANALYSIS METHODS

We review technical aspects of two-particle angular-correlation analysis methods applied to p - p collisions at the RHIC. Further method details appear in Refs. [4–6, 9, 10, 18, 20, 28–31].

A. Kinematic measures and spaces

High-energy nuclear collisions produce final-state hadrons as a distribution within cylindrical 3D momentum space (p_t, η, ϕ) , where p_t is transverse momentum, η is pseudorapidity and ϕ is azimuth angle. Transverse mass is $m_t = \sqrt{p_t^2 + m_h^2}$ with hadron mass m_h . Pseudorapidity is $\eta = -\ln[\tan(\theta/2)]$ (θ is polar angle relative to collision axis z), and $\eta \approx \cos(\theta)$ near $\eta = 0$. To improve visual access to low- p_t structure and simplify description of the p_t -spectrum hard component (defined below) we present spectra on transverse rapidity $y_t = \ln[(m_t + p_t)/m_h]$. For unidentified hadrons y_t , with pion mass assumed (about 80% of hadrons), serves as a regularized logarithmic p_t measure. A typical detector acceptance $p_t > 0.15$ GeV/c corresponds to $y_t > 1$.

Correlations are observed in two-particle momentum space $(p_{t1}, \eta_1, \phi_1, p_{t2}, \eta_2, \phi_2)$. An *autocorrelation* on angular subspace (x_1, x_2) (where $x = \eta$ or ϕ) is derived by averaging pair density $\rho(x_1, x_2)$ along diagonals on (x_1, x_2) parallel to the sum axis $x_\Sigma = x_1 + x_2$ [30]. The averaged pair density $\rho(x_\Delta)$ on defined *difference variable* $x_\Delta = x_1 - x_2$ is then an autocorrelation. The notation x_Δ

rather than Δx for difference variables is adopted to conform with mathematical notation conventions and to retain Δx as a measure of a detector acceptance on parameter x . For correlation structure approximately independent of x_Σ over some limited acceptance Δx (stationarity, typical over 2π azimuth and within some limited pseudorapidity acceptance $\Delta\eta$) angular correlations remain undistorted (no information is lost in the projection by averaging). p_t -integral 2D angular autocorrelations are thus lossless projections of 6D two-particle momentum space onto angle difference axes $(\eta_\Delta, \phi_\Delta)$. The ϕ_Δ axis is divided into *same-side* (SS, $|\phi_\Delta| < \pi/2$) and *away-side* (AS, $\pi/2 < |\phi_\Delta| < \pi$) intervals.

B. p-p initial-state geometry

For collisions between two composite projectiles the collision final state (FS) may depend on the transverse separation of the collision partners (impact parameter b) and the phase-space distribution of constituents within each projectile, collectively the initial-state (IS) geometry. We wish to determine how the IS geometry relates to an observable derived from FS hadrons and how the IS influences FS hadron yields, spectra and correlations.

For A - A collisions the projectile constituents are nucleons N all sharing a common lab velocity (modulo Fermi motion) and distributed over a nuclear volume. Based on a Glauber model of A - A collisions (assuming the eikonal approximation) nucleons are classified as participants (total number N_{part}) or spectators, and the mean number of N - N binary encounters N_{bin} is estimated. The relation $N_{bin} \sim N_{part}^{4/3}$ is a consequence of the eikonal approximation. Parameters N_{part} and N_{bin} , depending on A - A impact parameter b , are in turn related to macroscopic FS observable n_{ch} within some angular acceptance via the MB cross-section distribution $d\sigma(b)/dn_{ch}$.

For p - p collisions the constituents are partons distributed on the transverse configuration space of projectile protons *and* on longitudinal-momentum fraction x (fraction of proton momentum carried by a parton). One could apply a similar Glauber approach to p - p IS geometry, including assumed eikonal approximation as in the A - A description (e.g. default PYTHIA [15]). As noted in the introduction, it is conjectured that imposing a dijet trigger should favor more-central p - p collisions and therefore a substantial increase in soft-hadron production from low- x gluons [1]. However, some aspects of p - p collision data appear to be inconsistent with such a description, specifically parton transverse position and a p - p impact parameter. Nevertheless, FS measures for number of participant low- x partons and their binary encounters may be relevant and experimentally accessible [12].

C. p-p $y_t \times y_t$ and 2D angular correlations

$\rho(\vec{p}_1, \vec{p}_2)$ represents a basic pair density on 6D pair momentum space. The event-ensemble-averaged pair density $\bar{\rho}_{sib}$ derived from sibling pairs (pairs drawn from single events) includes the correlation structures to be measured. $\bar{\rho}_{mix}$ is a density of mixed pairs drawn from different but similar events. ρ_{ref} denotes a minimally-correlated reference-pair density derived from (a) a mixed-pair density or (b) a Cartesian product of SP angular densities $\bar{\rho}_0$ via a factorization assumption.

Differential correlation structure is determined by comparing a sibling-pair density to a reference-pair density in the form of difference $\Delta\rho = \bar{\rho}_{sib} - \rho_{ref}$ representing a correlated-pair density or *covariance* density. *Per-particle* measure $\Delta\rho/\sqrt{\rho_{ref}}$ has the form of Pearson's normalized covariance [32] wherein the numerator is a covariance and the denominator is approximately the geometric mean of marginal variances. In the Poisson limit a marginal variance may correspond to $\sigma_{n_{ch}}^2 \approx n_{ch} \propto \bar{\rho}_0$. Since $\rho_{ref} \approx \bar{\rho}_0 \times \bar{\rho}_0$ it follows that the geometric mean of variances is given by $\sqrt{\rho_{ref}} \approx \bar{\rho}_0$ and the normalized covariance density is a per-particle measure [30, 33, 34]. The number of final-state charged hadrons $\bar{\rho}_0 \sim n_{ch}$ in the denominator can be seen as a place holder. Other particle degrees of freedom may be more appropriate for various physical mechanisms (e.g. number of participant nucleons in A - A collisions, number of participant low- x partons in p - p collisions) as described below.

We define $\Delta\rho/\sqrt{\rho_{ref}} \equiv \bar{\rho}_0(r-1)$ where pair ratio $r \equiv \bar{\rho}_{sib}/\bar{\rho}_{mix}$ cancels instrumental effects. That per-particle measure is not based on a physical model. In some analyses a correlation amplitude is defined as $\bar{N}(r-1)$ with $\bar{N} \equiv \Delta\phi\Delta\eta\bar{\rho}_0$ [25], but such an amplitude then relies on a specific detector acceptance, is not ‘‘portable.’’

To assess the relation of data to IS geometry we convert per-charged-hadron model-fit results to $(2/N_{part})\Delta\rho = (2/N_{part})[\bar{\rho}_0^2(r-1)]$, the quantity in square brackets representing the *number of correlated pairs* within the detector acceptance. For this p - p analysis we assume the soft-component density $\bar{\rho}_s \equiv n_s/\Delta\eta$ is an estimator for p - p IS $N_{part}/2$ (low- x parton participants). Given the simplified notation $\Delta\rho/\sqrt{\rho_{ref}} \rightarrow A$ we plot $(\bar{\rho}_0/\bar{\rho}_s)A$ to convert ‘‘per-particle’’ from FS hadrons to IS low- x partons and obtain a more interpretable p - p per-particle measure.

Correlations on two-particle momentum space (\vec{p}_1, \vec{p}_2) can be factorized into distributions on 2D transverse-momentum space (p_{t1}, p_{t2}) or transverse-rapidity space $(y_{t1}, y_{t2}) \leftrightarrow y_t \times y_t$ [35] and on 4D angle space $(\eta_1, \phi_2, \eta_2, \phi_2)$ reducible with negligible information loss to autocorrelations on difference variables $(\eta_\Delta, \phi_\Delta)$ [20, 28, 30]. In this study we focus on minimum-bias (y_t -integral) 2D angular correlations. Each of the several features appearing in p - p 2D angular correlations (a correlation *component*) can be modeled within acceptance $\Delta\eta$ by a simple functional form (a model *element*), including 1D and 2D Gaussians and azimuth sinusoids uniform on η_Δ . The cosine elements $\cos(m\phi_\Delta)$ represent *cylindrical*

multipoles with pole number $2m$, e.g., dipole, quadrupole and sextupole for $m = 1, 2, 3$. Angular correlations can be formed separately for like-sign (LS) and unlike-sign (US) charge combinations, as well as for charge-independent (CI = LS + US) and charge-dependent (CD = LS - US) combinations [5, 6, 28, 29].

D. p-p nonjet azimuth quadrupole

The azimuth quadrupole ($m = 2$ Fourier) component is a prominent feature of A - A angular correlations, represented there by symbol $v_2 = \langle \cos(2\phi) \rangle$. The mean value is nominally relative to an estimated A - A reaction plane [36]. v_2 data are conventionally interpreted to represent elliptic flow, a hydrodynamic (hydro) response to IS asymmetry in non-central A - A collisions [37].

If 2D angular correlations are projected onto 1D azimuth *any* resulting distribution can be expressed exactly in terms of a Fourier series. The density of correlated pairs is then

$$\Delta\rho(\phi_\Delta) = \bar{\rho}_{sib} - \rho_{ref} = \Delta V_0^2 + 2 \sum_{m=1}^{\infty} V_m^2 \cos(m\phi_\Delta), \quad (1)$$

defining the *power-spectrum* elements V_m^2 of autocorrelation density $\Delta\rho(\phi_\Delta)$. The corresponding *per-pair* correlation measure is the ratio

$$\frac{\Delta\rho}{\rho_{ref}} = \Delta v_0^2 + 2 \sum_{m=1}^{\infty} v_m^2 \cos(m\phi_\Delta). \quad (2)$$

Some Fourier amplitudes from analysis of 1D azimuth projections may include contributions from more than one mechanism. For example, v_2 data from conventional 1D analysis may include contributions from jet-related (‘‘nonflow’’) as well as NJ (‘‘flow’’) mechanisms [7, 8]. In contrast, a complete model of 2D angular correlations *with η_Δ -dependent elements* permits isolation of several production mechanisms including a NJ quadrupole component [9, 10]. Fourier components from 2D correlation analysis are denoted by $V_m^2\{2D\}$ or $v_m^2\{2D\}$, and only the $m = 1$ and 2 (dipole and quadrupole) Fourier terms are *required* by 2D data histograms (see Sec. V) [20]. For measure $\Delta\rho/\sqrt{\rho_{ref}}$ data derived from model fits to 2D angular correlations the quadrupole component is denoted by $A_Q\{2D\} \equiv V_2^2\{2D\}/\bar{\rho}_0 = \bar{\rho}_0 v_2^2\{2D\}$ since the factorized reference density is $\rho_{ref} \rightarrow \bar{\rho}_0^2$.

In the present study of p - p 2D angular correlations we admit the possibility that a significant NJ quadrupole component may persist in high-energy p - p collisions (not necessarily of hydro origin) and retain the corresponding model element in the 2D data model function Eq. (6).

The measured p_t -integral NJ quadrupole data for Au-Au collisions are represented above 13 GeV by [9]

$$\begin{aligned} A_Q\{2D\}(b, \sqrt{s_{NN}}) &\equiv \bar{\rho}_0(b)v_2^2\{2D\}(b, \sqrt{s_{NN}}) & (3) \\ &= CR(\sqrt{s_{NN}})N_{bin}(b)\epsilon_{2,opt}^2(b), \end{aligned}$$

where $C = 4.5 \pm 0.2 \times 10^{-3}$, the energy-dependence factor is $R(\sqrt{s_{NN}}) = \log(\sqrt{s_{NN}}/13.5 \text{ GeV})/\log(200/13.5)$, N_{bin} is the estimated number of N - N binary encounters in the Glauber model, and $\epsilon_{2,opt}(b)$ is the Au-Au $m = 2$ overlap eccentricity assuming a continuous (optical-model) nuclear-matter distribution. Equation (3) describes measured y_t -integral azimuth quadrupole data in heavy ion collisions for all centralities down to N - N collisions and energies above $\sqrt{s_{NN}} \approx 13 \text{ GeV}$ and represents factorization of energy and centrality dependence for the NJ quadrupole. The 2D quadrupole data are also consistent with $V_2^2\{2D\} = \bar{\rho}_0 A_Q\{2D\} \propto N_{part} N_{bin} \epsilon_{2,opt}^2$ [7], a centrality trend that, modulo the IS eccentricity, *increases much faster than the dijet production rate*.

A non-zero value $v_2 \approx 0.02$ from Eq. (3) extrapolated to N - N collisions agrees with a p - p QCD color-dipole prediction [24]. As one aspect of the present p - p correlation study we confirm extrapolation of the Au-Au NJ quadrupole centrality trend to N - N collisions and determine the n_{ch} dependence of p - p $A_Q\{2D\}$. p - p NJ quadrupole systematics may help clarify the concept of p - p centrality: Is an IS eccentricity relevant for p - p collisions; if so how does it vary with n_{ch} ?

IV. TCM FOR p - p COLLISIONS

The two-component (soft+hard) model (TCM) of hadron production in high energy nuclear collisions has been reviewed in Refs. [4, 12] for p - p collisions and Refs. [18–20] for A - A collisions. The TCM serves first as a mathematical framework for data description and then, after comparisons with theory, as a basis for physical interpretation of data systematics. The TCM has been interpreted to represent two main sources of final-state hadrons: longitudinal projectile-nucleon dissociation (soft) and large-angle-scattered (transverse) parton fragmentation (hard). In A - A collisions the two processes scale respectively proportional to N_{part} (participant nucleons N) and N_{bin} (N - N binary encounters). Analogous scalings for p - p collisions were considered in Ref. [12].

The (soft + hard) TCM accurately describes most FS hadron yield and spectrum systematics [4, 18, 20], whereas there is no significant manifestation of the NJ quadrupole in yields and spectra [7, 8, 38]. In contrast, the NJ quadrupole plays a major role in A - A 2D angular correlations and is measurable as such even for p - p collisions (per this study). The TCM previously applied to yields and spectra must therefore be extended to include the NJ quadrupole as a third component of all high-energy nuclear collisions. An effective TCM should be complete and self-consistent, capable of describing all aspects of data from any collision system.

A. p - p single-particle y_t spectra

The joint single-charged-particle 2D (azimuth integral) density on y_t and η is denoted by $\rho_0(y_t, \eta) = d^2 n_{ch}/y_t dy_t d\eta$. The η -averaged (over $\Delta\eta$) y_t spectrum is $\bar{\rho}_0(y_t; \Delta\eta)$. The y_t -integral mean angular density is $\bar{\rho}_0(\Delta\eta) = \int dy_t y_t \bar{\rho}_0(y_t; \Delta\eta) \approx n_{ch}/\Delta\eta$ averaged over acceptance $\Delta\eta$ (η averages are considered in more detail in Sec. IX). The n_{ch} dependence of p - p y_t spectra was determined in Ref. [4], and MB spectra were decomposed into soft and hard components according to the TCM.

In p - p collisions soft and hard spectrum components have fixed forms but their relative admixture varies with n_{ch} [4]. The relation of the hard component to pQCD theory was established in Ref. [19]. In Au-Au collisions the soft component retains its fixed form but the hard-component form changes substantially with centrality, reflecting quantitative modification of jet formation [19]. Identification of the hard component with jets in p - p and more-peripheral Au-Au collisions is supported by data systematics and comparisons with pQCD theory [19, 21]. In more-central Au-Au collisions a jet interpretation for the TCM hard component has been questioned [20].

The two-component decomposition of p - p y_t spectra conditional on uncorrected n'_{ch} integrated over angular acceptance $\Delta\eta$ within 2π azimuth is denoted by [4]

$$\begin{aligned} \bar{\rho}_0(y_t; n'_{ch}) &= S(y_t; n'_{ch}) + H(y_t; n'_{ch}) \\ &= \bar{\rho}_s(n'_{ch}) \hat{S}_0(y_t) + \bar{\rho}_h(n'_{ch}) \hat{H}_0(y_t), \end{aligned} \quad (4)$$

where $\bar{\rho}_s = n_s/\Delta\eta$ and $\bar{\rho}_h = n_h/\Delta\eta$ are corresponding η -averaged soft and hard components with corrected $n_{ch} = n_s + n_h$ (see Sec. IX). The inferred soft and hard y_t spectrum shapes [unit normal $\hat{S}_0(y_t)$ and $\hat{H}_0(y_t)$] are independent of n'_{ch} and are just as defined in Refs. [18, 19]. The fixed hard-component spectrum shape $\hat{H}_0(y_t)$ (Gaussian plus power-law tail) is predicted quantitatively by measured fragmentation functions convoluted with a measured 200 GeV minimum-bias jet spectrum [19, 41].

Figure 1 (left) shows y_t spectra for several n'_{ch} classes. The spectra (uncorrected for tracking inefficiencies) are normalized by corrected-yield soft component $\bar{\rho}_s$. A common y_t -dependent inefficiency function is introduced for comparison of this analysis with corrected spectra in Ref. [4], indicated below $y_t = 2$ by the ratio of the two dash-dotted curves representing uncorrected $S'_0(y_t)$ and corrected $\hat{S}_0(y_t)$ soft-component models. The data spectra are represented by spline curves rather than individual points to emphasize systematic variation with n'_{ch} .

Figure 1 (right) shows normalized spectra from the left panel in the form $[\bar{\rho}'_0(y_t)/\bar{\rho}_s - S'_0(y_t)]/\bar{\rho}_s \approx \alpha \hat{H}_0(y_t)$ with $\alpha \approx 0.006$. From Ref. [4] we infer $\bar{\rho}_h \approx \alpha \bar{\rho}_s^2 = \alpha' \bar{\rho}'_s{}^2$. Given that empirical relation and $n'_{ch}/\Delta\eta \equiv \bar{\rho}'_0 = \bar{\rho}'_s + \bar{\rho}_h$ as simultaneous equations we can obtain $\bar{\rho}'_s$, $\bar{\rho}_s$ and $\bar{\rho}_h$ for any n'_{ch} and $\Delta\eta$ (see details in Sec. IX A). Note that although the data hard-component shapes for the lowest two n'_{ch} values deviate significantly from the $\alpha \hat{H}_0(y_t)$ model the integrals on y_t remain close to the value α .

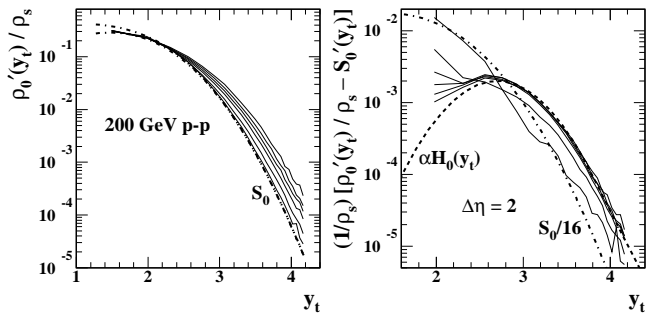


FIG. 1: Left: Normalized y_t spectra for six multiplicity classes of 200 GeV p - p collisions ($n = 1, \dots, 6$ see Table I). $\hat{S}_0(y_t)$ is the soft-component model function for corrected (upper dash-dotted) and uncorrected (lower dash-dotted) data. $\bar{\rho}_s$ is the soft-component multiplicity assuming $\alpha = 0.006$ (see text). The spectra are averaged over acceptance $\Delta\eta = 2$. Right: Spectrum hard components in the form $H(y_t)/\bar{\rho}_s^2$ from Eq. (4) compared to hard-component model function $\alpha\hat{H}_0(y_t)$ (dashed). Bars and carets are omitted from the figure labels.

The amplitude 0.33 of unit-normal \hat{H}_0 corresponds to the maximum of the dashed curve $0.006 \times 0.33 = 0.002$. These spectrum results are consistent with those from Ref. [4] with $\Delta\eta = 1$ (see Sec. IX D).

B. p - p dijet production

In Ref. [4] the TCM spectrum hard-component yield n_h within $\Delta\eta = 1$ was observed to vary as $n_h \approx 0.01n'_{ch}n_s$, with uncorrected $n'_{ch} \approx n_{ch}/2$. A refined analysis provided the more precise density relation $\bar{\rho}_h \approx \alpha\bar{\rho}_s^2$. As noted, the TCM soft-component density $\bar{\rho}_s$ is then defined by the simultaneous equations $\bar{\rho}_0 = \bar{\rho}_s + \bar{\rho}_h$, and $\bar{\rho}_h = \alpha\bar{\rho}_s^2$ for some $\alpha = O(0.01)$, consistent with pQCD plus Ref. [4]. In Ref. [12] $\bar{\rho}_s$ is associated with the number of *participant low- x partons* (gluons) and dijet production, proportional to the number of participant-parton binary encounters, is then observed to scale $\propto \bar{\rho}_s^2$.

Based on a dijet interpretation for the hard component we define $\bar{\rho}_h = n_h/\Delta\eta \equiv \epsilon(\Delta\eta)f(n'_{ch})2\bar{n}_{ch,j}$, where $f(n'_{ch})$ is the dijet frequency per collision and per unit η , $\epsilon(\Delta\eta) \in [0.5, 1]$ is the average fraction of a dijet appearing in acceptance $\Delta\eta$, and $2\bar{n}_{ch,j}$ is the MB mean dijet fragment multiplicity in 4π . Dijet fraction $\epsilon(\Delta\eta)$ should be distinguished from initial-state eccentricity $\epsilon_{2,opt}$ associated with the NJ quadrupole. We also distinguish among number of dijets, number of jets, dijet mean fragment multiplicity and jet mean fragment multiplicity (their values integrated over 4π vs within some limited detector acceptance $\Delta\eta$). The definition of $\bar{\rho}_h$ above separates factors $\epsilon \in [0.5, 1]$ and f that were combined in previous studies. The f values estimated here are thus approximately a factor 2 (i.e. $\approx 1/\epsilon$) larger than previous estimates [19, 21].

For 200 GeV NSD p - p collisions with $\bar{\rho}_s \approx 2.5$ and dijet mean fragment multiplicity $2\bar{n}_{ch,j} \approx 2.5 \pm 0.5$ derived

from measured jet systematics the inferred jet frequency $f_{NSD} = 0.006 \times 2.5^2/(0.55 \times 2.5) \approx 0.027$ is inferred from p - p spectrum data within $\Delta\eta = 1$. That value can be compared with the pQCD prediction $f_{NSD} = \sigma_{dijet}/(\sigma_{NSD}\Delta\eta_{4\pi}) \approx 4.5 \text{ mb}/(36.5 \text{ mb} \times 5) \approx 0.025$ for 200 GeV p - p collisions [19] based on a measured jet spectrum and NSD cross section corresponding to mean-value p - p parton distribution functions. Thus, the observed NSD p - p spectrum hard-component yield n_h [4] is quantitatively consistent with measured dijet systematics derived from event-wise jet reconstruction [39–41].

If a non-NSD p - p event sample with arbitrary mean n'_{ch} is selected we employ empirical n_{ch} trends consistent with Ref. [4] and having their own pQCD implications, as discussed in Ref. [12]. We assume for the present study that the dijet frequency varies with soft multiplicity as

$$f(n'_{ch}) \approx 0.027 \left[\frac{\bar{\rho}_s(n'_{ch})}{\bar{\rho}_{s,NSD}} \right]^2 \quad (5)$$

with $\bar{\rho}_{s,NSD} = 2.5$ for 200 GeV p - p collisions. We define $n_j(n'_{ch}) = \Delta\eta f(n'_{ch})$ as the *dijet number* within some angular acceptance $\Delta\eta$. For the n'_{ch} range considered in this study the fraction of hard hadrons n_h/n_{ch} is not more than about 15%. The p - p final state is never dominated by hard processes but MB dijet production does play a major role, especially for $y_t < 3.3$ ($p_t < 2 \text{ GeV}/c$) where *most jet fragments appear*.

C. p - p two-particle correlations

MB two-particle correlations have been studied extensively for NSD p - p collisions [5, 6, 31] and Au-Au collisions [20, 28, 35]. A correspondence between jet-related correlations and y_t -spectrum hard components has been established quantitatively in Refs. [5, 6, 21]. p - p angular-correlation structure is consistent with extrapolation of the centrality systematics of angular correlations from Au-Au collisions [20]. Both correlations on transverse rapidity $y_t \times y_t$ and 2D angular correlations on $(\eta_\Delta, \phi_\Delta)$ from p - p collisions are described by the TCM. $y_t \times y_t$ correlations for 200 GeV p - p collisions are fully consistent with the SP y_t spectrum results described above and in Ref. [4]. The hard component corresponds (when projected onto 1D y_t) to the hard component of Eq. (4).

Figure 2 (left panel) shows $y_t \times y_t$ correlations for 200 GeV approximately NSD p - p collisions. The logarithmic interval $y_t \in [1, 4.5]$ corresponds to $p_t \in [0.15, 6] \text{ GeV}/c$. The two peak features correspond to TCM soft and hard components. The 2D hard component with mode near $y_t = 2.7$ ($\approx 1 \text{ GeV}/c$) corresponds quantitatively to the 1D SP spectrum hard component modeled by $\hat{H}_0(y_t)$ in Ref. [4]. The soft component (US pairs only) is consistent with longitudinal fragmentation (dissociation) of projectile nucleons manifesting local charge conservation.

Figure 2 (right panel) shows 2D angular correlations on difference variables $(\eta_\Delta, \phi_\Delta)$. The hadron p_t values

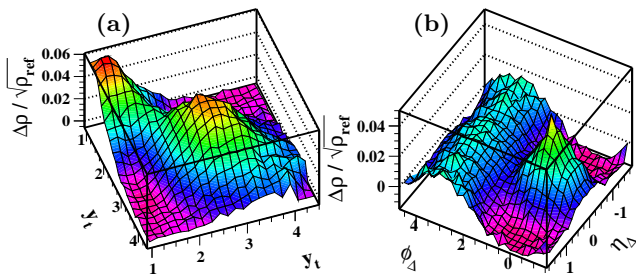


FIG. 2: (Color online) (a) Minimum-bias correlated-pair density on 2D transverse-rapidity space $y_t \times y_t$ from 200 GeV p - p collisions showing soft (smaller y_t) and hard (larger y_t) components as peak structures. (b) Correlated-pair density on 2D angular difference space $(\eta_\Delta, \phi_\Delta)$. Hadrons are selected with $p_t \approx 0.6$ GeV/c ($y_t \approx 2$). Nevertheless, features expected for dijets are observed: (i) same-side 2D peak representing intrajet correlations and (ii) away-side 1D peak on azimuth representing interjet (back-to-back jet) correlations [5, 6].

for that plot are constrained to lie near 0.6 GeV/c (just above $y_t = 2$), corresponding to the saddle between soft and hard peaks in the left panel. Although the hadron p_t is very low the structures expected for jet angular correlations are still clearly evident: a SS 2D peak at the origin representing intrajet correlations and a 1D peak on azimuth at $\phi_\Delta = \pi$ corresponding to interjet correlations between back-to-back jet pairs. The volume of the SS 2D peak corresponds quantitatively to the hard component of the total hadron yield inferred from y_t spectrum data and to pQCD calculations [21]. The soft component, a narrow 1D Gaussian on η_Δ including only US charge pairs, is excluded by the $p_t > 0.5$ GeV/c cut [6].

Angular correlation systematics have been compared to the QCD Monte Carlo PYTHIA [15], and general qualitative agreement is observed [5]. The correlation measure $\Delta\rho/\sqrt{\rho_{ref}}$ proportional to the number of correlated pairs per final-state hadron [20] is analogous to ratio n_h/n_s given $n_h \rightarrow$ correlated-pair number. In the present study we extend the p - p results by measuring systematic variations of 2D angular correlations with parameter n'_{ch} .

V. p - p 2D ANGULAR CORRELATIONS

Two-particle angular correlations are obtained with the same basic methods as employed in Refs. [4, 8, 20, 28]. Data for this analysis were obtained from a MB sample of p - p collisions at $\sqrt{s} = 200$ GeV. Charged particles were detected with the STAR Time Projection Chamber (TPC). The acceptance was 2π azimuth, pseudorapidity $|\eta| < 1$, and $p_t > 0.15$ GeV/c. The *observed* (uncorrected) charge multiplicity within the η acceptance is denoted by n'_{ch} , whereas the efficiency-corrected and p_t -extrapolated *true* event multiplicity in the acceptance is denoted by n_{ch} with corrected mean angular density $\bar{\rho}_0 = n_{ch}/\Delta\eta$ within acceptance $\Delta\eta$. Seven event classes indexed by the observed charged-particle multiplicity are

defined in Table I. The range of corrected particle density $\bar{\rho}_0(n'_{ch})$ is approximately 2-20 particles per unit η . This analysis is based on 6 million (M) events, compared to 3M events for the p_t -spectrum study in Ref. [4].

TABLE I: Multiplicity classes based on the observed (uncorrected) multiplicity n'_{ch} falling within acceptance $|\eta| < 1$ or $\Delta\eta = 2$. The efficiency-corrected density is $\bar{\rho}_0 = n_{ch}/\Delta\eta$. Event numbers are given in millions (M = 1×10^6). TCM parameters include $\alpha = 0.006$ and $\xi = 0.6$.

Class n	1	2	3	4	5	6	7
n'_{ch}	2-3	4-6	7-9	10-12	13-17	18-24	25-50
$\langle n'_{ch} \rangle$	2.52	4.87	7.81	10.8	14.3	19.6	26.8
$\bar{\rho}_0(n'_{ch})$	1.76	3.41	5.47	7.56	10.0	13.7	18.8
Events (M)	2.31	2.21	0.91	0.33	0.14	0.02	0.001

Table I shows the multiplicity classes and numbers of events per class from 6M p - p events, with charge multiplicity averaged over acceptance $|\eta| < 1$ or $\Delta\eta = 2$. The first row presents the bins defined on observed (uncorrected) multiplicity n'_{ch} within $\Delta\eta$. The second row presents uncorrected event-number-weighted bin means. The third row presents efficiency- and p_t -acceptance-corrected mean densities on η , with correction factor ≈ 1.6 . Those multiplicity classes extend over a 11:1 ratio range compared with 12:1 for the RHIC p - p analysis in Ref. [4] and 7.6:1 for the LHC analysis in Ref. [25].

The approximately 2.25M events in each of the first two multiplicity bins can be compared with 0.12M events for the 10% most-peripheral centrality bin from a correlation analysis of 200 GeV Au-Au collisions in Ref. [20]. The 2D histogram per-bin statistical uncertainties for the present study are more than 4.5 times smaller. Histograms for the first five p - p bins each have better statistics than a 200 GeV Au-Au histogram from Ref. [20].

Figure 3 shows 2D histograms for the first six multiplicity bins. The histograms are corrected for y_t and angle-averaged inefficiencies. The correlation measure is $\Delta\rho/\sqrt{\rho_{ref}} \equiv \bar{\rho}_0(\bar{\rho}_{sib}/\bar{\rho}_{mix} - 1)$ with prefactor $\bar{\rho}_0$ corrected [20]. These are p_t -integral or MB angular correlations with no p_t “trigger” condition. The 2D histograms are binned 25×25 on $(\eta_\Delta, \phi_\Delta)$ as for the analyses in Refs. [20, 28]. The pair acceptance on η_Δ (accepted interval on η_Σ) falls linearly from a maximum at the origin to $1/25$ that value at the outermost bins. The outermost bins (at $|\eta_\Delta| \approx 2$) are not shown in the figure because statistical fluctuations there distract from the significant correlation structure in other bins.

The prominent correlation features are a 1D peak on η_Δ , a SS 2D peak at the origin and an AS 1D peak at π on ϕ_Δ . The amplitudes of the last two features appear to increase with n_{ch} much more rapidly than that of the first feature. The SS 2D peak structure is actually a superposition of a broader jet-related peak (mainly US pairs) and a narrower composite peak including Bose-Einstein correlations (BEC, LS pairs) and gamma-conversion electrons (US pairs) [5, 6]. Visual evidence for a significant

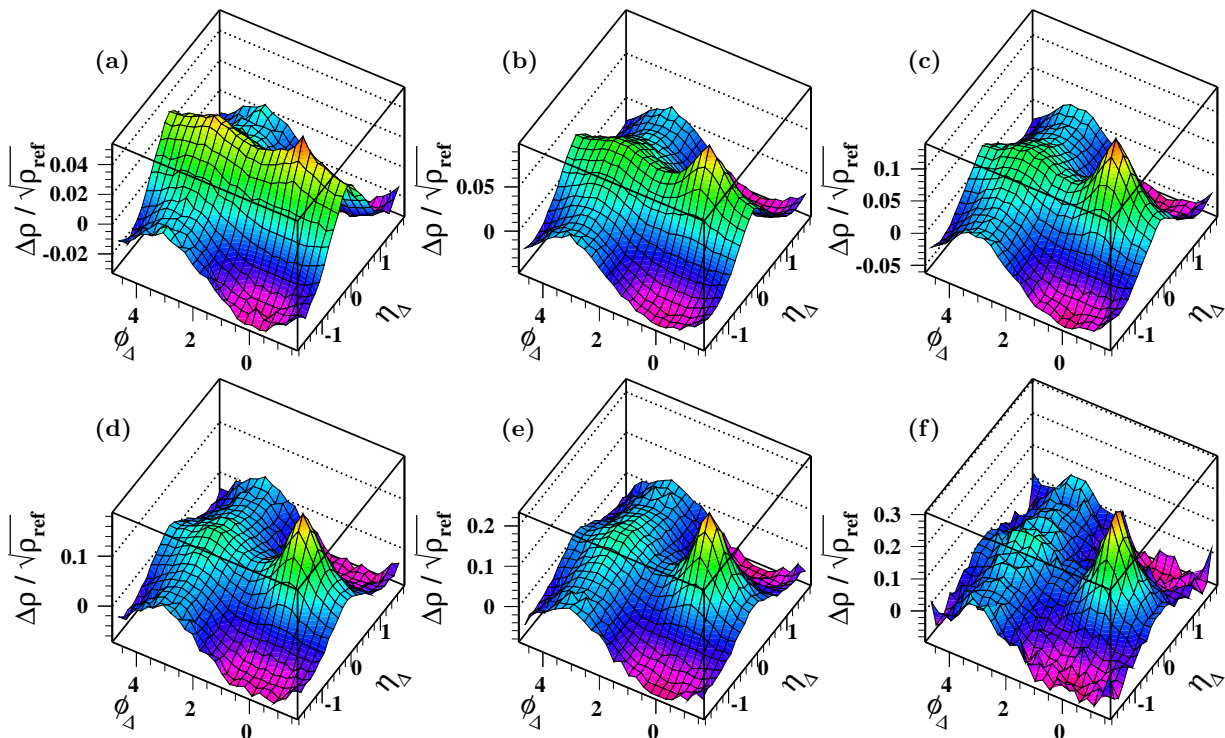


FIG. 3: (Color online) Evolution of y_t -integral charge-independent 2D angular correlations as $\Delta\rho/\sqrt{\rho_{\text{ref}}} \equiv \bar{\rho}_0(\bar{\rho}_{\text{sib}}/\bar{\rho}_{\text{mix}} - 1)$ on $(\eta_\Delta, \phi_\Delta)$ with n'_{ch} (see Table I) for p - p collisions at $\sqrt{s} = 200$ GeV averaged over acceptance $\Delta\eta = 2$. The pair ratio in the measure definition cancels instrumental effects and $\bar{\rho}_0$ is corrected for single-particle inefficiencies.

NJ quadrupole component is also apparent in the figure, as discussed in Sec. VIB.

VI. 2D MODEL FITS

Model fits to 2D angular correlations can provide an accurate quantitative description of 2D histogram data. The fit model resolves several correlation components subsequently interpreted to represent distinct hadron production mechanisms. In this section we apply the eleven-parameter fit model from Refs. [5, 6, 20, 28].

A. 2D model function

2D angular-correlation histograms are fitted with a *six-element model function*, the simplest model that provides a reasonable description of all minimum-bias p - p data and Au-Au data for all centralities [4, 8, 20, 28]. This “standard” model was motivated by the simple features apparent in the 2D correlation histograms, not by *a priori* physical assumptions [5, 6]. A $\cos(2\phi_\Delta)$ azimuth quadrupole component required to describe Au-Au data is retained in the p - p fit model for the present study.

The 2D model function on $(\eta_\Delta, \phi_\Delta)$ employed for this analysis includes (i) a SS 2D Gaussian, (ii) an η_Δ -independent AS azimuth dipole $\cos(\phi_\Delta - \pi)$, (iii) an η_Δ -

independent azimuth quadrupole $\cos(2\phi_\Delta)$, (iv) a ϕ_Δ -independent 1D Gaussian on η_Δ , (v) a SS 2D exponential and (vi) a constant offset. The 2D fit model is then the sum of the six elements

$$\begin{aligned} \frac{\Delta\rho}{\sqrt{\rho_{\text{ref}}}} = & A_0 + A_{2D} \exp\left\{-\frac{1}{2}\left[\left(\frac{\phi_\Delta}{\sigma_{\phi_\Delta}}\right)^2 + \left(\frac{\eta_\Delta}{\sigma_{\eta_\Delta}}\right)^2\right]\right\} \\ & + A_D \{1 + \cos(\phi_\Delta - \pi)\}/2 + A_{BEC,e-e}(\eta_\Delta, \phi_\Delta) \\ & + A_Q 2 \cos(2\phi_\Delta) + A_{\text{soft}} \exp\left\{-\frac{1}{2}\left(\frac{\eta_\Delta}{\sigma_{\text{soft}}}\right)^2\right\}, \quad (6) \end{aligned}$$

the same eleven-parameter model used to describe MB Au-Au angular correlations in Ref. [20]. The symmetrized 25×25 -bin data histograms include more than 150 degrees of freedom and strongly constrain the model parameters. Based on measured parameter trends and comparisons with QCD theory elements (i) and (ii) together have been attributed to dijet production [20], (iii) is conventionally identified with elliptic flow in A - A collisions [13, 36, 42]), (iv) is attributed to projectile-nucleon dissociation and element (v) models BEC and conversion-electron pairs.

Equation (6) differs from the model in Refs. [12, 20] where the dipole and quadrupole terms are expressed as $A_D \cos(\phi_\Delta - \pi)$ and $A_Q \cos(2\phi_\Delta)$. The form of the dipole term in Eq. (6) is the limiting case (with increasing peak width) of a periodic AS 1D peak array [43]. Note that in Fig. 3 the SS 2D peak is fully resolved on η_Δ in all cases.

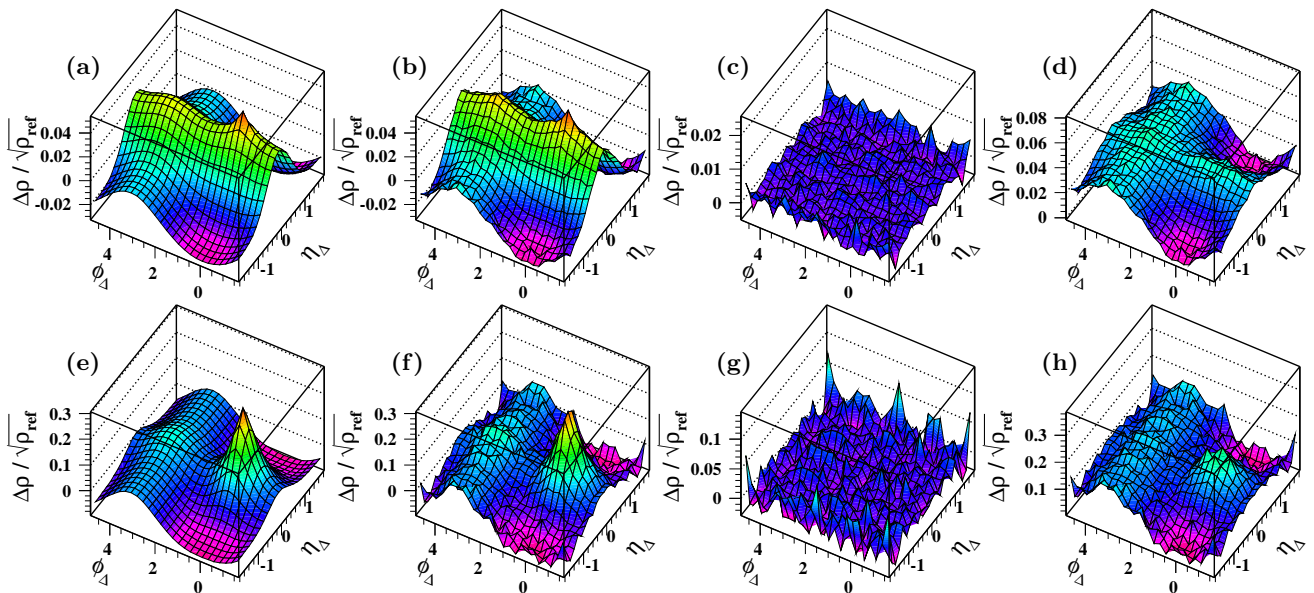


FIG. 4: (Color online) Perspective views of charge-independent, y_t -integral 2D angular correlations as $\Delta\rho/\sqrt{\rho_{ref}}$ on $(\eta_\Delta, \phi_\Delta)$ from p - p collisions at $\sqrt{s} = 200$ GeV for $n = 1, 6$ multiplicity classes (upper and lower rows respectively). (a,e) fit model, (b,f) data histogram, (c,g) fit residuals (vertical sensitivity increased two-fold), (d,h) jet + NJ quadrupole contributions obtained by subtracting fitted offset, soft-component and BEC/electron elements of the fit model from the data histograms (see text).

The $m = 1, 2$ multipoles (AS dipole, NJ quadrupole) are then the only other significant structures on azimuth ϕ_Δ .

B. Model-fit results

Fig. 4 shows examples of fit decomposition and residuals using data from the first (upper row) and sixth (lower row) multiplicity bins. The two rows show (left to right) model fit, data, residuals (data–model) and jet-related + NJ quadrupole structure. The last are obtained by subtracting fitted model elements soft (iv), BE/electrons (v) and offset (vi) from the data histograms leaving jet-related structure (i), (ii) and NJ quadrupole (iii). Residuals (c) and (g) (those plots are a factor 2 more sensitive) are comparable in magnitude to statistical errors and negligible compared to the amplitudes of the principal correlation features. The lack of significant nonrandom structure in the residuals suggests that the standard fit model exhausts all information in the data. For comparison purposes panels (d) and (h) are plotted with the same vertical intervals as data histograms (b) and (f), but the fitted offsets (vi) have been subtracted.

Figures 5 and 6 show fit-parameter trends vs corrected multiplicity density $n_{ch}/\Delta\eta = \bar{\rho}_0$. Best-fit descriptions of the data histograms were obtained with a χ^2 minimization procedure. The general trends with increasing n_{ch} are: (a) *per-particle* SS 2D and AS 1D peak amplitudes increase approximately linearly with n_{ch} , (b) the NJ quadrupole amplitude increases approximately as n_{ch}^2 and (c) the soft-component amplitude remains constant. The SS-peak *per-particle* amplitude increases nearly ten-

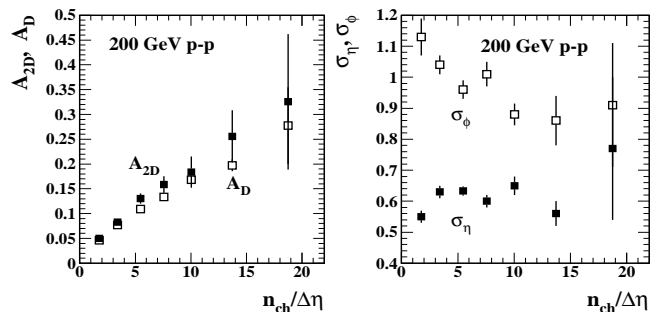


FIG. 5: Left: SS 2D peak and AS 1D dipole amplitudes A_{2D} and A_D vs corrected charge density $\bar{\rho}_0 = n_{ch}/\Delta\eta$. Right: SS 2D peak η and ϕ widths vs charge density.

fold with similar increase of n_{ch} , consistent with the spectrum hard-component scaling trend reported in Ref. [4].

The SS 2D peak remains *strongly elongated on azimuth* even for larger multiplicities (aspect ratio drops from 2:1 to 1.5:1) in contrast to strong elongation on η in more-central Au-Au collisions [20, 28]. The width of the soft-component 1D peak on η_Δ is $\sigma_{soft} = 0.47 \pm 0.02$, comparable to the η_Δ width of the SS 2D peak $\sigma_{\eta_\Delta} \approx 0.6$. The correlated *pair number* from the BEC part of the SS peak is expected to scale quadratically with n_{ch} . The per-particle BEC amplitude should then increase approximately linearly with n_{ch} , similar to observed jet-related correlations from p - p collisions. That expectation is consistent with the data in Fig. 3.

Visible manifestations of the rapidly-increasing NJ quadrupole amplitude are apparent in Fig. 4. The SS

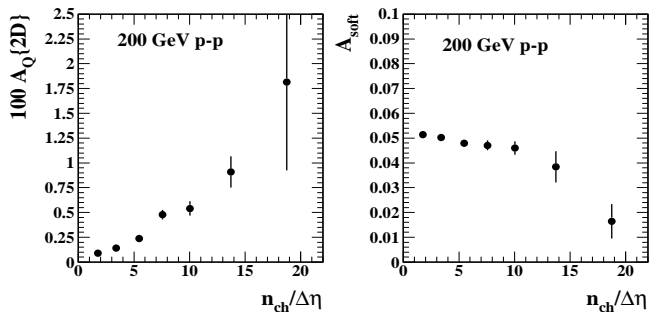


FIG. 6: Left: NJ quadrupole amplitude $A_Q\{2D\} \equiv \bar{\rho}_0 v_2^2\{2D\}$ vs corrected charge density. Right: Soft-component 1D Gaussian (on η_Δ) amplitude A_{soft} vs charge density.

azimuth curvature within $|\eta_\Delta| > 1$ at $\phi_\Delta = 0$ is substantially positive in (b) or (d) but becomes negligible in (f) or (h), whereas the negative AS curvature near $\phi_\Delta = \pi$ approximately doubles with n_{ch} . The combined trends are expected with the presence of an increasing azimuth quadrupole component. The relation between NJ quadrupole, AS dipole and resulting SS curvature is discussed further in Sec. XI in connection with the SS “ridge” observed in LHC p - p angular correlations for certain cut conditions, as first reported in Ref. [25].

To summarize, the per-particle phenomenology of 2D angular correlations vs n_{ch} for 200 GeV p - p collisions as in Fig. 3 includes three main components (soft, hard, NJ quadrupole) exhibiting simple trends with n_{ch} : (a) The soft-component amplitude remains approximately constant, (b) the hard-component (jet-related) amplitudes increase linearly, and (c) the NJ quadrupole amplitude increases quadratically and becomes visually apparent for larger n_{ch} . We first examine the jet-related trends in the context of the TCM and pQCD dijet production, then consider two NJ components and extend the TCM to include the NJ quadrupole component.

VII. JET-RELATED CORRELATIONS

We combine pQCD predictions for minimum-bias dijet production in NSD p - p collisions from Ref. [19] with an n_{ch} trend inferred from spectrum data in Ref. [4] and the relation between spectrum yields and jet-related angular correlations established in Ref. [21] to predict jet-related angular-correlation trends for 200 GeV p - p collisions. We consider components (i) and (ii) of 2D angular correlations as described in Sec. VIA. The plotted quantities are per-hadron correlation measures A_X converted to per-participant-parton measures by the added factor $n_{ch}/n_s = \bar{\rho}_0(\Delta\eta)/\bar{\rho}_s(\Delta\eta)$ assuming $\bar{\rho}_s$ represents participant low- x partons (gluons).

A. Predicting dijet correlations

In terms of per-particle correlation measure $\Delta\rho/\sqrt{\rho_{ref}}$ the volume of the SS 2D peak averaged over the angular acceptance ($\Delta\eta, \Delta\phi$) is represented by [21]

$$J^2/\rho_0 = \bar{\rho}_0 j^2(b) \equiv \frac{2\pi\sigma_\eta\sigma_\phi A_{2D}}{2\pi\Delta\eta}, \quad (7)$$

with $j^2 = 2\epsilon(\Delta\eta) n_j \overline{n_{ch,j}^2(\Delta\eta)}/\overline{n_{ch}(n_{ch}-1)}$ as an event-wise pair ratio (number of correlated pairs over total number of pairs in some acceptance) [21]. Equation (7) is a per-particle measure of jet-correlated pairs from all jets within the angular acceptance. The factor $2\epsilon(\Delta\eta)$ (≈ 1.3 for $\Delta\eta = 2$) includes the probability that the recoil partner jet of a dijet also appears within $\Delta\eta$ [21].

The volume of the SS 2D peak modeled as a 2D Gaussian is represented by $V_{SS2D} = 2\pi\sigma_\eta\sigma_\phi A_{2D}$. The SS peak volume includes any n_{ch} dependence of the peak widths and is thus a more direct measure of jet fragment yields than A_{2D} . The results above can be combined to obtain

$$\begin{aligned} V_{SS2D} &= 2\pi\Delta\eta\bar{\rho}_0 j^2 = n_{ch} j^2 \\ &= n_{ch} 2\epsilon(\Delta\eta) n_j (n_{ch}) \frac{\overline{n_{ch,j}^2}}{n_{ch}^2}. \end{aligned} \quad (8)$$

The per-participant-parton measure is then

$$\begin{aligned} \frac{n_{ch}}{n_s} V_{SS2D} &= 2\epsilon n_j \overline{n_{ch,j}^2} \times 1/n_s \\ &= 2\epsilon(\Delta\eta) f_{NSD} \frac{\overline{n_{ch,j}^2}(\Delta\eta)}{\bar{\rho}_{s,NSD}^2} G^2(\Delta\eta) \bar{\rho}_s \end{aligned} \quad (9)$$

where $O(1)$ factor $G^2 = \overline{n_{ch,j}^2}/\bar{n}_{ch,j}^2$ accounts for fluctuations in the jet fragment multiplicity (see App. C of Ref. [21]), and we have used the expression for $f(n'_{ch}) = n_j(n'_{ch})/\Delta\eta$ in Eq. (5) including a value for f_{NSD} consistent with event-wise-reconstructed jet data.

B. Data trends for jet-related correlations

Factor n_{ch}/n_s applied to fitted correlation amplitudes from histograms in Fig. 3 in the context of Ref. [12] converts from per-charged-hadron to per-participant-parton measures, analogous to factor $2n_{ch}/N_{part}$ applied to spectra in A - A analysis [18]. We then plot renormalized amplitudes vs $\bar{\rho}_s$ to test the relation predicted by Eq. (9).

Figure 7 (left panel) shows per-participant jet-related SS 2D peak volume vs soft multiplicity density $n_s/\Delta\eta = \bar{\rho}_s$. The solid squares are V_{SS2D} derived from SS peak amplitude A_{2D} combined with measured widths σ_{η_Δ} and σ_{ϕ_Δ} from Fig. 5. The open square is derived from analysis of 200 GeV Au-Au collisions [20]. The 84-93% centrality bin approximates MB N - N collisions.

The dash-dotted line represents Eq. (9) (second line) with mean fragment multiplicity $\bar{n}_{ch,j} = 3.3$ and fluctuation parameter $G^2 = 1.5$. The fragment multiplicity is

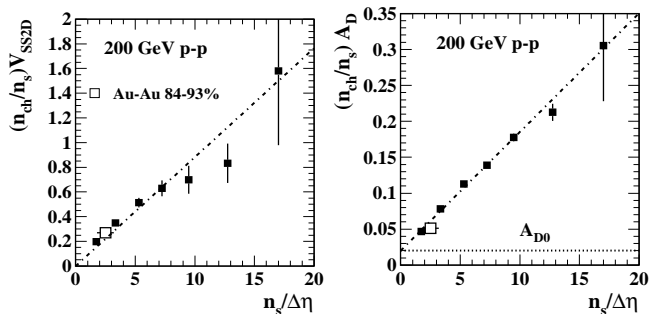


FIG. 7: Left: SS peak volume V_{SS2D} rescaled by factor n_{ch}/n_s to per-participant form (for $\Delta\eta = 2$) vs soft-component density $\bar{\rho}_s \equiv n_s/\Delta\eta$. Right: Rescaled AS dipole amplitude A_D vs soft-component density. Constant offset A_{D0} is expected for global transverse-momentum conservation. Open boxes represent peripheral Au-Au data equivalent to N - N collisions.

scaled up from value 2.2 inferred for $\Delta\eta = 1$ in Ref. [4] based on simulations that indicate a 50% jet fragment detection efficiency for $\Delta\eta = 1$ and 75% efficiency for $\Delta\eta = 2$ (acceptance-edge losses). The fluctuation parameter value is Poisson value 1.3 for $\bar{n}_{ch,j} = 3.3$ plus an estimated additional contribution from non-Poisson fluctuations (see Ref. [21], App. A). The other factors are $f_{NSD} = 0.027$ from Sec. IV B and $2\epsilon = 1.25$ for $\Delta\eta = 2$.

Figure 7 (right panel) shows per-participant amplitudes for the AS 1D peak (solid squares) interpreted to represent back-to-back jet pairs. Since the AS 1D peak has a fixed geometry and represents a fixed fraction of the dijet number we expect $A_D \propto V_{SS2D}$ modulo small offset A_{D0} representing global transverse-momentum conservation that is expected to be independent of η acceptance and/or charged-particle number [20]. The dashed line is Eq. (9) times factor 1/5 adjusted to accommodate the A_D data, confirming that $A_D \propto V_{SS2D}$ within data uncertainties modulo fixed offset $A_{D0} \approx 0.02$.

VIII. NONJET CORRELATIONS

The nonjet components of 2D angular correlations correspond to three model elements described in Sec. VI A: (iii) the NJ azimuth quadrupole, (iv) a 1D peak on η_Δ attributed to projectile nucleon dissociation and (v) a contribution to the SS 2D peak from BEC and conversion electron pairs. The last is not relevant to this study except as a possible source of systematic error. The first two are considered in this section. As above, the plotted quantities are per-hadron correlation measures A_X converted to per-participant-parton measures by added factor $n_{ch}/n_s = \bar{\rho}_0(\Delta\eta)/\bar{\rho}_s(\Delta\eta)$.

A. Predicting the NJ azimuth quadrupole

For Au-Au collisions we observe the following centrality trend for the NJ quadrupole (number of correlated pairs) valid over a large energy interval above 13 GeV [9]

$$V_2^2(b) = \bar{\rho}_0(b)A_Q(b) \propto N_{part}(b)N_{bin}(b)\epsilon_{opt}^2(b), \quad (10)$$

where for A - A collisions $N_{bin} \propto N_{part}^{4/3}$ is a manifestation of the eikonal approximation within the Glauber model.

For p - p collisions we find that, relative to the soft hadron density $\bar{\rho}_s$, dijet production scales $\propto \bar{\rho}_s^2$ as described in Sec. IV B. We then argue by analogy with A - A systematics that for p - p collisions $N_{part} \sim \bar{\rho}_s$ and dijets $\propto N_{bin} \propto N_{part}^2 \sim \bar{\rho}_s^2$ (the eikonal approximation is not valid). The corresponding form of Eq. (10) for the NJ quadrupole in p - p collisions should then be

$$V_2^2(n'_{ch}) = \bar{\rho}_0(n'_{ch})A_Q(n'_{ch}) \propto N_{part}^3\langle\epsilon^2\rangle, \quad (11)$$

since there is apparently no systematic dependence on impact parameter b and therefore no b -dependent $\epsilon(b)$. With $N_{part} \sim \bar{\rho}_s$ we then obtain

$$V_2^2(n'_{ch})/\bar{\rho}_s = (\bar{\rho}_0/\bar{\rho}_s)A_Q(n'_{ch}) \propto \bar{\rho}_s^2 \quad (12)$$

as a *predicted* trend for the NJ quadrupole in p - p collisions based on measured Au-Au quadrupole systematics and the assumption that *the NJ azimuth quadrupole is a universal feature of all high-energy nuclear collisions*.

B. Data trends for nonjet correlations

Figure 8 (left panel) shows fitted NJ quadrupole amplitude $A_Q\{2D\} = \bar{\rho}_0 v_2^2\{2D\}$ rescaled to a per-participant-parton quantity by factor $\bar{\rho}_0/\bar{\rho}_s = n_{ch}/n_s$. The dashed curve is

$$(\bar{\rho}_0/\bar{\rho}_s)100A_Q\{2D\} = (0.075\bar{\rho}_s)^2 + 0.07 \quad (13)$$

indicating that the data (modulo small fixed offset A_{Q0}) are consistent with a quadratic dependence on $\bar{\rho}_s$ in contrast to the linear dependence for jet production in Fig. 7. The open square is an extrapolation from 200 GeV Au-Au data based on the empirical relation $A_Q\{2D\} = 0.0045N_{bin}\epsilon_{opt}^2$ [9]. For the peripheral Au-Au limit $\epsilon_{opt} \approx 0.4$ and $N_{bin} = 1$ for N - $N \approx$ NSD p - p collisions give $100A_Q\{2D\} \approx 0.07$, in quantitative agreement with p - p data (relative to empirical offset $100A_{Q0} = 0.07$). The offsets A_{D0} and A_{Q0} for dipole and quadrupole components are consistent with global transverse-momentum conservation [20]. The per-participant trend in Fig. 8 (left panel) increases 100-fold over the measured n_{ch} interval, and the same quadratic trend on $\bar{\rho}_s$ continues down to zero hadron density inconsistent with a collective (flow) phenomenon resulting from particle rescattering.

Figure 8 (right panel) shows the per-participant soft-component amplitude $(\bar{\rho}_0/\bar{\rho}_s)A_{soft}$. Within uncertainties the per-participant amplitude is constant over most

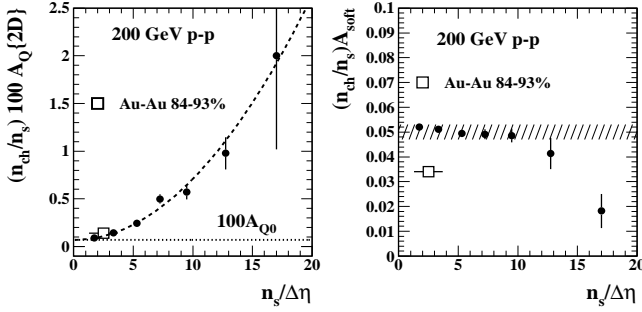


FIG. 8: Left: Rescaled NJ quadrupole amplitude $100A_Q$ vs soft-component charge density. Offset $100A_{Q0}$ may be an aspect of global transverse-momentum conservation. Right: Rescaled soft-component amplitude A_{soft} vs soft-component charge density. The open boxes represent peripheral Au-Au data equivalent to MB N - N collisions.

of the plotted interval as expected for correlated-pair number from projectile dissociation $\propto \bar{\rho}_s$. That trend is consistent with models in which a charged hadron from projectile dissociation may be correlated with one other nearest-neighbor charged hadron, per string fragmentation models and local parton-hadron duality [44]: Nearest-neighbor hadrons are correlated as charge-neutral pairs satisfying local charge and momentum conservation.

The trends of the principal p - p correlation components can be summarized as follows (as correlated pairs vs participants): the soft component scales as $\bar{\rho}_s \propto N_{\text{part}}$, the hard (dijet) component scales as $f \propto N_{\text{bin}} \sim N_{\text{part}}^2$, and the NJ quadrupole scales as $V_2^2 \propto N_{\text{part}}N_{\text{bin}} \sim N_{\text{part}}^3$. In other analysis it was determined that the SS 2D jet peak represented by A_{2D} is comprised mainly of US pairs, whereas the NJ quadrupole in Au-Au collisions is CI (LS = US) [5, 6]. And the NJ quadrupole and MB dijets have different n_{ch} trends. These measurements confirm a revised *three*-component model for p - p angular correlations in which the NJ quadrupole plays a unique role.

IX. TCM FOR η -DENSITY DISTRIBUTIONS

Section IV describes the TCM for p - p y_t spectra in the form of Eq. (4), a marginal projection onto y_t of the 2D hadron density on (y_t, η) . In this section we consider the complementary marginal projection onto η and derive a TCM for the η density in terms of averages over a detector acceptance $\Delta\eta$. Given y_t -spectrum results we expect a correspondence between the TCM hard component on η and the distribution of low- x gluons within the proton.

A. Relation to y_t spectra and TCM

Hadron production integrated over azimuth can be represented by SP joint density $\rho_0(y_t, \eta)$. Given results from

the spectrum analysis in Ref. [4] we assume as a basic TCM decomposition the first line of

$$\begin{aligned} \rho_0(y_t, \eta; n'_{ch}) &= S(y_t, \eta; n'_{ch}) + H(y_t, \eta; n'_{ch}) \quad (14) \\ &\approx \rho_{s0}(n'_{ch})S_0(\eta)\hat{S}_0(y_t) \\ &\quad + \rho_{h0}(n'_{ch})H_0(\eta)\hat{H}_0(y_t). \end{aligned}$$

The second line of Eq. (14) invokes factorization of both soft and hard components as in Eq. (4). We assume that soft component $S(y_t, \eta; n'_{ch})$ is factorizable within some limited acceptance $\Delta\eta$ consistent with projectile dissociation modeled by string fragmentation. Hard component $H(y_t, \eta; n'_{ch})$ may include significant η - y_t covariances owing to details of dijet production (strong variation of dijet production with η). We assume factorization here and consider deviations in Sec. IX D. Spectrum model functions $\hat{S}_0(y_t)$ and $\hat{H}_0(y_t)$ on y_t were defined in Sec. IV A as in Ref. [4] and are unit integral (indicated by carets) *over the full y_t acceptance*. Model functions $S_0(\eta)$ and $H_0(\eta)$ on η are newly defined below, and the ρ_{x0} represent soft- and hard-component hadron densities at $\eta = 0$.

In Ref. [4] $\rho_0(y_t, \eta; n'_{ch})$ was averaged over acceptance $\Delta\eta = 1$ to obtain a y_t spectrum TCM described by

$$\begin{aligned} \bar{\rho}_0(y_t; n'_{ch}, \Delta\eta) &\approx \bar{\rho}_s(n'_{ch}, \Delta\eta)\hat{S}_0(y_t) \quad (15) \\ &\quad + \bar{\rho}_h(n'_{ch}, \Delta\eta)\hat{H}_0(y_t), \end{aligned}$$

where $\bar{\rho}_x(n'_{ch}, \Delta\eta) \equiv n_x/\Delta\eta$ with $x = s, h$ and bars indicate averages over η . That model describes corrected and extrapolated y_t spectra. In general, the effects of spectrum low- y_t inefficiency and a y_t acceptance cutoff must be represented by TCM model functions (compare upper and lower dash-dotted curves in Fig. 1 – left). Because inferred hard-component model $\hat{H}_0(y_t)$ is negligible below 0.35 GeV/c we assume that low- y_t inefficiencies and cutoff affect only soft components of yields and spectra. We replace unit-integral $\hat{S}_0(y_t)$ (upper) in Eq. (14) with modified soft-component model function $S'_0(y_t)$ (lower) and define soft-component tracking efficiency

$$\xi \equiv \int_0^\infty dy_t y_t S'_0(y_t) \leq 1 \quad (16)$$

implying $\rho'_{s0}(n'_{ch}) = \xi\rho_{s0}(n'_{ch})$. For the present y_t -integral study we integrate $\rho'_0(y_t, \eta; n'_{ch})$ over y_t to obtain

$$\rho'_0(\eta; n'_{ch}) \approx \rho'_{s0}(n'_{ch})S_0(\eta) + \rho_{h0}(n'_{ch})H_0(\eta), \quad (17)$$

where $S_0(\eta)$ and $H_0(\eta)$ are TCM model functions with unit amplitude at $\eta = 0$, and primes indicate the effect of low- y_t acceptance limits and inefficiencies.

Averaging Eq. (17) over some acceptance $\Delta\eta$ symmetric about $\eta = 0$ gives

$$\begin{aligned} \bar{\rho}'_0(n'_{ch}, \Delta\eta) &= \rho'_{s0}(n'_{ch})\bar{S}_0(\Delta\eta) + \rho_{h0}(n'_{ch})\bar{H}_0(\Delta\eta) \\ &\equiv \bar{\rho}'_s(n'_{ch}, \Delta\eta) + \bar{\rho}_h(n'_{ch}, \Delta\eta), \quad (18) \end{aligned}$$

with mean values $\bar{\rho}_x(n'_{ch}, \Delta\eta) = n_x/\Delta\eta = \rho_{x0}\bar{X}_0(\Delta\eta)$. The TCM of Eq. (17) can then be rewritten in the form

$$\begin{aligned} \rho'_0(\eta; n'_{ch}) &\approx \bar{\rho}'_s(n'_{ch}, \Delta\eta)\tilde{S}_0(\eta; \Delta\eta) \quad (19) \\ &\quad + \bar{\rho}_h(n'_{ch}, \Delta\eta)\tilde{H}_0(\eta; \Delta\eta) \end{aligned}$$

with $\bar{\rho}'_s(n'_{ch}, \Delta\eta)$ and $\bar{\rho}_h(n'_{ch}, \Delta\eta)$ inferred from n'_{ch} based on an assumed value for parameter α' or α as discussed below. The $\tilde{X}_0(\eta; \Delta\eta)$ (denoted by a tilde) have average value 1 over acceptance $\Delta\eta$ by definition. Averaging Eq. (19) over the η acceptance should then be consistent with integration of Eq. (15) over the y_t acceptance (above the y_t cutoff) provided that $\hat{S}_0(y_t)$ is replaced by $S'_0(y_t)$.

As in Sec. IV A we must define a value for parameter α or α' to determine the decomposition of $\bar{\rho}_0$ into $\bar{\rho}_h$ and $\bar{\rho}_s$ or $\bar{\rho}'_s$. We impose a TCM constraint that with increasing index n'_{ch} no part of $\bar{\rho}_s$ -normalized data distributions should decrease, establishing a lower limit for α . For y_t spectra that condition requires a soft component varying approximately as $\bar{\rho}_s \approx \bar{\rho}_0 - \alpha\bar{\rho}_0^2$ [4]. A self-consistent analysis leads to $\bar{\rho}_h(n'_{ch}, \Delta\eta) \approx \alpha(\Delta\eta)\bar{\rho}_s^2(n'_{ch}, \Delta\eta)$ for corrected y_t spectra, with $\alpha(\Delta\eta = 1) \approx 0.006$ as inferred in Ref. [4]. In the present study we define $\alpha'(\Delta\eta) = \bar{\rho}_h/\bar{\rho}_s^2 = \alpha(\Delta\eta)/\xi^2$ to accommodate a soft-component y_t cutoff and low- y_t tracking inefficiency. That condition plus $\bar{\rho}'_0 = \bar{\rho}'_s + \bar{\rho}_h$ define a quadratic equation from which n'_s or $\bar{\rho}'_s = n'_s/\Delta\eta$ can be inferred for any uncorrected n'_{ch} or $\bar{\rho}'_0$ given a fixed value for α' or α and efficiency ξ .

B. Corrected pseudorapidity densities

Uncorrected SP η densities have the form

$$\frac{dn'_{ch}}{d\eta} = [1 + g(\eta)]\lambda(\eta)\rho'_0(\eta; n'_{ch}), \quad (20)$$

where $g(\eta)$ in the first factor represents a common instrumental distortion antisymmetric about $\eta = 0$ affecting both TCM components in common. The undistorted density $\rho'_0(\eta; n'_{ch})$ is assumed to be symmetric about $\eta = 0$ given the symmetric p - p collision system. Those assumptions permit isolation of $g(\eta)$ for each n'_{ch} value.

Figure 9 (left) shows measured density distributions $dn'_{ch}/d\eta$ normalized by uncorrected soft component $\bar{\rho}'_s = n'_s/\Delta\eta$ for several multiplicity classes assuming $\alpha = 0.012$ with efficiency and y_t -acceptance factor $\xi = 0.6$. An η -symmetric inefficiency $\lambda(\eta) \leq 1$ is observed to deviate from unity only for the outer two bins on each end of the η acceptance, with values 0.925 and 0.993 for $|\eta| = 0.95$ and 0.85 respectively. The plotted data are corrected for $\lambda(\eta)$ but a common η -asymmetric distortion remains.

Figure 9 (right) shows asymmetric data distributions divided by their η -symmetrized counterparts revealing the common η -asymmetric instrumental distortion $g(\eta)$. The dashed model curve through the points is $1 + g(\eta) = 1 - 0.044 \tanh(7\eta)$. The model points at $\eta = \pm 0.95$ are then shifted up and down by 0.008 relative to that trend. The correction is independent of n'_{ch} within statistics. Such an asymmetry is expected if tracking efficiencies in two halves of the TPC differ by a few percent owing to readout-electronics malfunctions. The slope near $\eta = 0$ reflects the primary-vertex distribution on the z axis.

Figure 10 (left) shows the asymmetry-corrected normalized densities $\rho'_0(\eta; n'_{ch})/\bar{\rho}'_s(n'_{ch})$ (points). The solid

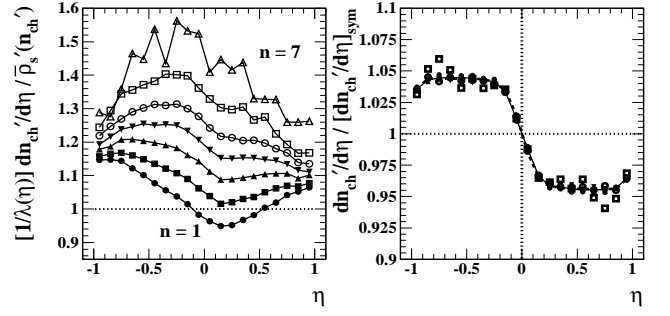


FIG. 9: Left: Uncorrected η densities within $\Delta\eta = 2$ for seven multiplicity classes (see Table I). The curves connecting data points guide the eye. Right: Ratios of data at left to symmetrized versions revealing a common instrumental asymmetry modeled by the dashed curve. (data for $n = 7$ are omitted for clarity).

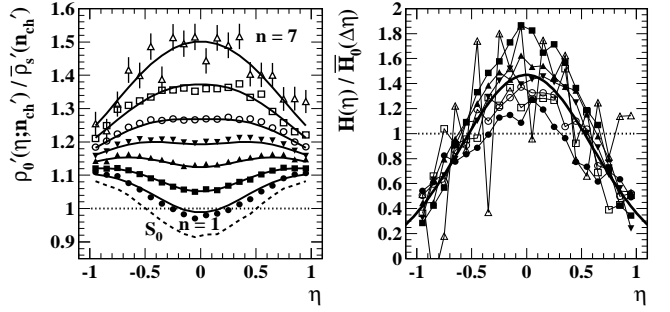


FIG. 10: Left: Corrected η densities within $\Delta\eta = 2$ for seven multiplicity classes. The dashed curve is normalized soft-component model $\tilde{S}_0(\eta) \equiv S_0(\eta)/\tilde{S}_0(\Delta\eta)$ from Eq. (24). The solid curves are Eq. (19) with TCM elements defined in Eqs. (24) and (22). Right: Data hard components inferred as in Eq. (21). The solid curve is normalized hard-component model $\tilde{H}_0(\eta)$ as defined in Eq. (22).

curves through the data are defined by Eq. (19) with soft and hard model functions defined below. The dashed curve is $\tilde{S}_0(\eta)$ defined in Eq. (24), the soft-component limit to the ratio $\rho'_0(\eta)/\bar{\rho}'_s$ as $n'_{ch} \rightarrow 0$.

C. Inferring the pseudorapidity density TCM

The TCM soft and hard model functions can be isolated by the following strategy based on Eq. (19). Differences between successive ratios $\rho'_0(\eta; n'_{ch})/\bar{\rho}'_s(n'_{ch})$ (data sets in Fig. 10 - left panel) should cancel common term $\tilde{S}_0(\eta)$ leaving terms approximated by $(\bar{\rho}_{h,n}/\bar{\rho}'_{s,n} - \bar{\rho}_{h,n-1}/\bar{\rho}'_{s,n-1})\tilde{H}_0(\eta)$. The difference data are divided by the factor in parenthesis to obtain estimates for the form of hard-component model $\tilde{H}_0(\eta)$ which are described by a Gaussian function. $\tilde{H}_0(\eta)$ is then used to infer $\tilde{S}_0(\eta)$.

Figure 10 (right) shows data difference distributions

$$\frac{H_n(\eta)}{\tilde{H}_0(\Delta\eta)} \equiv \frac{\rho'_0(\eta)_n/\bar{\rho}'_{s,n} - \rho'_0(\eta)_{n-1}/\bar{\rho}'_{s,n-1}}{\bar{\rho}_{h,n}/\bar{\rho}'_{s,n} - \bar{\rho}_{h,n-1}/\bar{\rho}'_{s,n-1}}, \quad (21)$$

where index $n \in [1, 7]$ represents the seven multiplicity classes. As noted, the difference in the numerator cancels common term $\tilde{S}_0(\eta; \Delta\eta)$ (defined below). For $n = 1$ we assume $\rho'_0(\eta)_{n-1}/\bar{\rho}'_{s,n-1} \rightarrow \tilde{S}_0(\eta; \Delta\eta)$, and $\bar{\rho}_{h,n}/\bar{\rho}'_{s,n} - \bar{\rho}_{h,n-1}/\bar{\rho}'_{s,n-1} \rightarrow \bar{\rho}_{h,1}/\bar{\rho}'_{s,1}$ (i.e. the extrapolation to $n = 0$ is assumed to be pure soft component). Given the TCM of Eq. (19) that expression should represent a common hard-component model in the form $H_0(\eta)/\bar{H}_0(\Delta\eta)$. The inferred model function for $\Delta\eta = 2$ (bold solid curve) is

$$\tilde{H}_0(\eta; \Delta\eta) \equiv \frac{H_0(\eta)}{\bar{H}_0(\Delta\eta)} = 1.47 \exp[-(\eta/0.6)^2/2], (22)$$

where $\sqrt{2\pi\sigma^2} \approx 1.47$ for $\sigma = 0.6$ (the Gaussian tails are truncated) and the normalized function is denoted by a tilde. The hard-component form is, within statistical errors, approximately independent of n_{ch} over an interval implying a 100-fold increase in dijet production, suggesting that most of the hard-component yield (MB dijet fragments) falls within the acceptance $\Delta\eta = 2$.

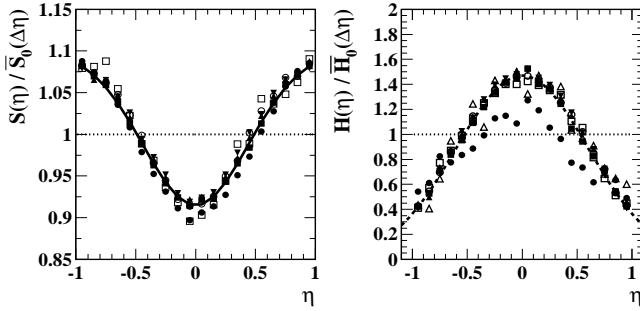


FIG. 11: Left: Data soft components inferred as in Eq. (23). The solid curve is normalized soft-component model $\tilde{S}_0(\eta)$ as defined in Eq. (24). Right: Data hard components inferred as in Eq. (25). The solid curve is normalized hard-component model $\tilde{H}_0(\eta)$ as defined in Eq. (22). The data for $n = 1$ (solid dots) are significantly low compared to the common trend.

Figure 11 (left) shows the soft-component estimator

$$\frac{S_n(\eta)}{\tilde{S}_0(\Delta\eta)} \equiv \frac{\rho'_0(\eta)_n/\bar{\rho}'_{s,n} - (\bar{\rho}_{h,n}/\bar{\rho}'_{s,n})\tilde{H}_0(\eta; \Delta\eta)}{\tilde{S}_0(\Delta\eta)}, (23)$$

with $\tilde{H}_0(\eta; \Delta\eta)$ as defined in Eq. (22). The inferred soft-component model for $\Delta\eta = 2$ (solid curve) is defined by

$$\tilde{S}_0(\eta; \Delta\eta) \equiv \frac{S_0(\eta)}{\tilde{S}_0(\Delta\eta)} = 1.09 - 0.18 \exp[-(\eta/0.44)^2/2]. (24)$$

The form of the soft component also appears to be invariant over a large n_{ch} interval. The small data deviations from the model are consistent with statistical errors. The minimum at $\eta = 0$ is expected given the Jacobian for $\eta \leftrightarrow y_z$, where an approximately uniform distribution on y_z is expected within a limited Δy_z acceptance.

Figure 11 (right) shows the hard component estimated from data with an alternative method assuming $\tilde{S}_0(\eta)$

$$\frac{H_n(\eta)}{\bar{H}_0(\Delta\eta)} \equiv \frac{\rho'_0(\eta)_n/\bar{\rho}'_{s,n} - \tilde{S}_0(\eta; \Delta\eta)}{\bar{\rho}_{h,n}/\bar{\rho}'_{s,n}}, (25)$$

which substantially reduces statistical noise in the differences. The dashed curve is the hard-component model $\tilde{H}_0(\eta; \Delta\eta)$ defined in Eq. (22) confirming TCM self-consistency. The points for $n = 1$ (solid dots) are low compared to the general trend, which may indicate that the hard component for $n = 1$ extends sufficiently low on y_t to be significantly reduced by the low- y_t tracking inefficiency and acceptance cutoff (see Fig. 1 – right).

The hard-component density in the right panel suggests that hadron fragments from MB dijets are strongly peaked near $\eta = 0$, mainly within $\Delta\eta = 2$ consistent with the dominant dijet source being low- x gluons corresponding to small y_z or η . The functional form on η is also consistent with the “gluon-gluon source” component described in Ref. [45]. The energy dependence $N_{ch}^{gg} \propto \ln^3(s_{NN}/s_0)$ of the integrated gluon-gluon source noted there may arise in p - p (N - N) collisions from the $\bar{\rho}_h \propto \bar{\rho}_s^2$ trend derived from Ref. [4] and the present measurements, from the $\bar{\rho}_s \propto \ln(\sqrt{s}/10 \text{ GeV})$ energy trend noted in Ref. [20], and from 4π integration over η (y_z) that introduces an additional $\ln(\sqrt{s}/10 \text{ GeV})$ factor.

D. y_t spectrum η -acceptance dependence

We now consider the effect on the y_t spectrum of varying $\Delta\eta$. As noted below Eq. (14) there is reason to expect some η dependence for the y_t -spectrum hard component due to the low- x structure of projectile protons (rapid increase of the gluon density with decreasing x). Here we present hard components extracted within $\Delta\eta = 1$ and 2 to address that question. We assume that $\tilde{S}_0(y_t)$ does not vary significantly within $\Delta\eta = 2$.

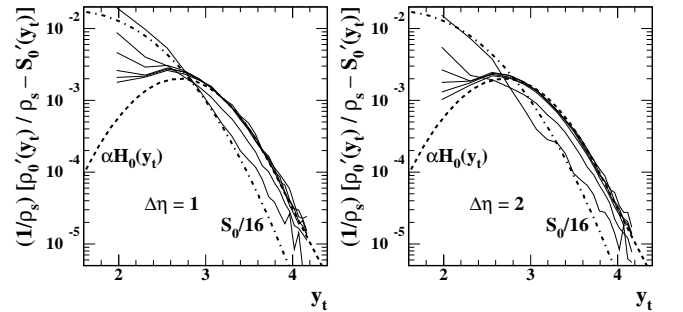


FIG. 12: Comparison of inferred spectrum hard components for $\Delta\eta = 1$ (left) and $\Delta\eta = 2$ (right) demonstrating the increased yield at smaller y_t for the smaller η acceptance. That result is consistent with the hard-component density in Fig. 11 (right) assuming correspondence with dijets from low- x partons (gluons) as the source for the spectrum hard component.

Figure 12 shows inferred spectrum hard components in the form $H(y_t)/\bar{\rho}_s^2$ for two values of acceptance $\Delta\eta$. The dashed curves show fixed hard-component model function $\alpha\tilde{H}_0(y_t)$ (Gaussian with power-law tail) for comparison. The densities $\bar{\rho}_0$, $\bar{\rho}_s$, $\bar{\rho}_h$ are derived within $\Delta\eta = 2$ for both cases. Above $y_t = 3$ ($p_t \approx 1.4 \text{ GeV}/c$) the dis-

tributions are equivalent for all multiplicity classes.

Below $y_t = 3$ the y_t -spectrum hard component increases substantially within the smaller η acceptance, nearer the peak of $\tilde{H}_0(\eta)$. The increase near $y_t = 2$ ($p_t \approx 0.5$ GeV/c) is a factor 2. That trend can be understood as follows: Near $\eta = 0$ an increased MB dijet fragment yield is expected at lower y_t because more lower- x participant gluons are favored there, and the lowest-energy jets ($E_{jet} \approx 3$ GeV) may have FFs skewed to lower fragment momenta. At larger η larger- x partons are favored, and the higher-energy jets have harder FFs.

For the lowest multiplicity class the hard component falls mainly below $y_t = 2.7$ ($p_t \approx 1$ GeV/c) and may continue to increase below 0.5 GeV/c. That trend is consistent with the corresponding data in Fig. 11 (right) that fall well below the trend for other multiplicity classes.

X. SYSTEMATIC UNCERTAINTIES

We consider uncertainties in TCM decomposition of charge multiplicity n_{ch} and SP y_t spectra and η densities. We demonstrate that the standard 2D fit model is a necessary and sufficient model for p - p angular correlations. And we consider uncertainties in jet-related and NJ quadrupole systematics resulting from 2D model fits.

A. Integrated-multiplicity systematics

Decomposition of corrected n_{ch} within acceptance $\Delta\eta$ into soft and hard components n_s and n_h based on uncorrected yield n'_{ch} relies on estimation of efficiency ξ and coefficient α (Sec. IX A). Efficiency is determined via Eq. (16) by integrating soft model $S'_0(y_t)$ that describes uncorrected spectrum data to obtain $\xi \approx 0.6$ reflecting a combination of low- y_t tracking inefficiency and y_t acceptance cutoff. The estimated value in Ref. [4] was $\xi = 0.5$ with slightly higher p_t cutoff (0.20 vs 0.15 GeV/c).

The estimated value for α differs between y_t spectra and η densities. In the former case $\alpha \approx 0.006$, in the latter $\alpha \approx 0.012$. The relevant value is within $\alpha \in 0.01 \pm 0.005$ but with significant systematic bias depending on the context. We speculate that the lower value for y_t spectra describes well the region $y_t > 2.7$ ($p_t > 1$ GeV/c) where the hard-component shape is the same for all n_{ch} , but not the region below that point where the shape is strongly dependent on n_{ch} and substantially exceeds $H_0(y_t)$. In contrast, the density on η integrates over the entire y_t acceptance and includes those extra contributions, requiring a larger value for α .

B. Single-particle y_t spectra and η densities

Definition of the soft component is a central issue for TCM decomposition. The soft component is defined as the limiting case of ratio $\rho_0/\bar{\rho}_s$ as $\bar{\rho}_s \rightarrow 0$. If Eq. (4)

or Eq. (19) does describe corresponding data the fixed soft component $S_0(y_t)$ or $S_0(\eta)$ should emerge as a stable limiting case, and that is what we observe. Subtraction of the soft-component model reveals a stable hard-component shape with exception of two low- n_{ch} hard components where deviations occur mainly at lower y_t .

For the η densities in Sec. IX, Fig. 11 indicates that the TCM system is self-consistent at the level of statistical error with the exception of the lowest n_{ch} class. That exception is likely due to bias toward lowest-energy jets near mid-rapidity (for small n_{ch} condition) where the mean fragment distribution extends down into the inefficient low- y_t region as shown in Fig. 12. One indication of self-consistency is the opposite trends on η of soft and hard components in Fig. 11 suggesting minimal crosstalk.

Uncertainties in the TCM for y_t spectra are discussed at length in Ref. [4]. Uncertainty in the soft component increases substantially below $y_t \approx 2.5$ ($p_t \approx 0.8$ GeV/c), but the hard component falls off sharply below that point, with apparent lower bound for p - p collisions near $y_t = 1.6$ ($p_t \approx 0.35$ GeV/c). Thus, the hard-component absolute magnitude near and above its mode is well-defined, and n_{ch} dependence below that point relative to the fixed soft component remains informative.

C. Necessary and sufficient 2D fit model

Although the standard 2D fit model in Eq. (6) applied to Au-Au data provides an excellent overall description of those 2D histograms [20] its uniqueness may be questioned. For instance, is a specific data component divided among two or more model elements (jet peak and “ridge”), do multiple data components contribute to a single model element (“flow” and “nonflow”), are additional model elements required to describe some data (e.g. “higher harmonics”)?

Those questions have been addressed in several studies. Arguments against “higher harmonics” based on extensive data analysis are presented in Refs. [46, 47]. A comparison of several candidate 1D fit models based on Bayesian inference methods in Ref. [48] demonstrates that a 1D projection of the standard 2D fit model is overwhelmingly preferred over other candidates (e.g. Fourier series). A recent study demonstrates that 1D models based on Fourier series confuse contributions from two sources of azimuth quadrupole structure (“flow” and “nonflow”) [8].

In the present study we apply the standard model for A - A collisions to p - p data although the quadrupole model element is not *required* by MB p - p correlation data (A_Q is not significant for the lowest multiplicity class). However, the n_{ch} trend from this study makes clear that a NJ quadrupole element is definitely required for larger n_{ch} values. The standard 2D fit model is thus established as *necessary* for these p - p data, and the fit residuals demonstrate that the standard model is *sufficient* (all fit residuals are consistent with statistical errors, see Fig. 4).

D. Jet-related systematics

Four correlation components have substantial amplitudes near the angular origin: the SS 2D jet peak, the soft component, conversion-electron pairs and BEC. There is thus a potential near the origin for cross-talk among correlation components and model elements, especially since dijet and BEC pair numbers have the same quadratic trend on n_{ch} . Charge combinations combined with correlation shapes and p_t dependence permit distinctions.

The jet-related SS 2D peak corresponds mainly to US pairs (local charge conservation during parton fragmentation). BEC modeled by a 2D exponential relates only to LS pairs. Conversion electron pairs relate only to US pairs but the peak is very narrow. The soft component (nearly uniform on ϕ_Δ) relates only to US pairs. Distinctions among correlation components based on their charge properties have been explored in Refs. [5, 6].

Jet-related components are almost completely separated from soft and BEC/electron components respectively above and below $p_t \approx 0.5$ GeV/c (Fig. 2). However, for y_t -integral studies (as in the present case) there may be some cross talk between SS 2D peak and soft component depending on their relative amplitudes. And the BEC/electron peak may contribute a small fixed fractional bias to the SS 2D jet peak independent of n_{ch} .

The major covariances are between the SS peak ϕ width and the soft component (Fig. 5, right), and between soft and SS 2D peak amplitudes (Fig. 6, right, last point). The AS 1D peak (AS dipole) is immune to SS peak covariances and may be used as a reference for dijet production. The SS 2D peak volume and AS 1D amplitude should scale together with n_{ch} reflecting the common n_j dijet production trend, and that correlation is confirmed in Fig. 7.

E. NJ quadrupole systematics

The relevance of a NJ quadrupole component for 200 GeV p - p collisions may be questioned, especially for the MB case. In modeling a jet-related AS 1D peak there is ambiguity between a 1D Gaussian or a combination of dipole and quadrupole multipoles (as in the standard 2D model). For a sufficiently broad AS peak the two models may be equivalent, and any quadrupole component inferred from the standard 2D model could be jet-related.

However, what we observe in Fig. 8 (left) is equivalent to a cubic trend on ρ_s for the NJ quadrupole pair number, distinct from the quadratic trend observed for jet-related spectrum and correlation components. And the cubic trend for the quadrupole in p - p collisions ($\propto N_{part}N_{bin}$) is comparable to the trend observed for the NJ quadrupole in Au-Au collisions ($\propto N_{part}N_{bin}\epsilon_{opt}^2$) where other factors argue for a unique NJ quadrupole component [8]. Thus, we conclude that the NJ quadrupole inferred for p - p collisions from the standard 2D model is significant and signals the presence of a unique quadrupole mecha-

nism in elementary collisions. While such a mechanism is evidently “collective” in the sense that it involves the correlated motion of multiple FS hadrons, its interpretation in terms of hydrodynamic flow as a result of particle rescattering in a small transient system is questionable.

XI. LHC p - p “RIDGE” AND SS CURVATURES

Three manifestations of so-called “ridge” phenomena reported at the RHIC and LHC can be distinguished: (i) η elongation of a monolithic SS 2D jet peak in A - A collisions well described by a single 2D Gaussian [20, 28], (ii) claimed development of a separate η -uniform ridge-like structure beneath a symmetric 2D jet peak also in A - A collisions [49], and (iii) appearance of an SS ridge in p - p collisions for certain kinematic cut conditions [11, 25]. Item (i) is well established for untriggered (no p_t cuts) jet correlations but has been referred to as a “soft ridge” [22, 50], although there is no separate ridge per se distinguished from the SS 2D jet peak. Item (ii) appears for certain combinations of p_t cuts (“triggered” jet analysis) and may also be jet-related.

We refer here to item (iii)—the so-called “CMS ridge.” Appearance of a SS ridge in CMS data for some cut combinations might be associated with item (ii) above, given the apparent similarity. However, the absence of η elongation as in (i) and consistency with measured NJ quadrupole systematics makes interpretation (ii) unlikely. There is no indication from this study that the CMS ridge is directly associated with the SS 2D jet peak.

A study in Ref. [11] demonstrated that extrapolation of NJ quadrupole trends from Au-Au data to N - N (p - p) collisions and from RHIC to LHC energies could account quantitatively for the observed CMS ridge. One motivation for the present study has been confirmation of a significant NJ quadrupole amplitude in p - p collisions and determination of its n_{ch} dependence. We now relate that new information to the CMS ridge phenomenon.

A. Azimuth curvatures and the “ridge” phenomena

Given the properties of 2D angular correlations from p - p collisions as reported in this study, structure such as the SS ridge reported by CMS for 7 TeV p - p data [25] may result from competition between two curvatures on ϕ_Δ within $|\eta_\Delta| > 1$ (which excludes most of the SS 2D jet peak). A SS ridge may appear when azimuth structure near $\phi_\Delta = 0$ in that region becomes significantly concave downward (negative *net* curvature). For MB p - p collisions only positive net curvatures appear, but a small *relative* change in certain correlation amplitudes may result in qualitative appearance or disappearance of a ridge.

As reported in Sec. VI the dominant structures within $|\eta_\Delta| > 1$ are the AS dipole sinusoid $\cos(\phi_\Delta - \pi)$ and the azimuth quadrupole sinusoid $\cos(2\phi_\Delta)$. At a point where the slope of a function $f(x)$ is zero its curvature k is just

the second derivative $k = f''(x)$. The curvature at a maximum is negative. The curvatures of the cylindrical multipoles $\cos[m(\phi - \pi)]$ at $\phi = 0$ are $(-1)^{m+1}m^2$. The curvature of $\cos(2\phi_\Delta)$ at $\phi_\Delta = 0$ is then four times the curvature of $\cos(\phi_\Delta - \pi)$ and with opposite sign.

Absolute curvatures are determined by the coefficients of the two sinusoids $-A_D/2$ for dipole and $2A_Q$ for quadrupole. In defining the separate curvatures we include a common factor $\bar{\rho}_0/\bar{\rho}_s$ to take advantage of the simple trends in Figs. 7 (right) and 8 (left). The curvatures for dipole and quadrupole respectively are then $k_D = (\bar{\rho}_0/\bar{\rho}_s)A_D/2$ and $k_Q = -8(\bar{\rho}_0/\bar{\rho}_s)A_Q$. Zero net curvature corresponds to $4 \times 2A_Q = A_D/2$ or $-k_Q/k_D = 16A_Q/A_D = 1$. A ridge (negative net curvature) may be identified if that ratio is significantly greater than one.

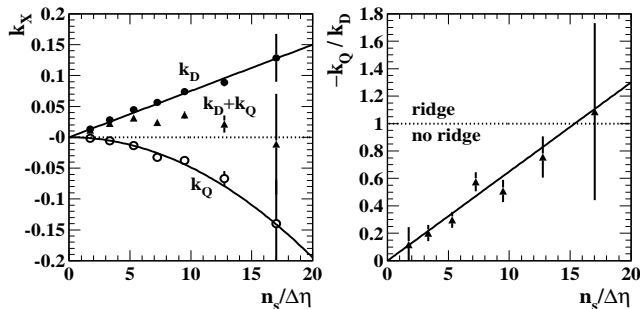


FIG. 13: Left: Azimuth curvatures k_D and k_Q for dipole and quadrupole components respectively and net curvature $k_D + k_Q$, all evaluated at $\phi_\Delta = 0$. Right: Curvature ratio $-k_Q/k_D$ that predicts when a SS “ridge” will appear within $|\eta_\Delta| > 1$ at $\phi_\Delta = 0$.

Figure 13 (left) shows curvatures k_X at $\phi_\Delta = 0$ vs soft density $\bar{\rho}_s$ (proxy for number of participant low- x gluons). The net curvature $k_D + k_Q$ (solid triangles) is also shown. As determined by the trends in Figs. 7 (right) and 8 (left) the dipole curvature is positive and increases linearly while the quadrupole curvature is negative and increases (in magnitude) quadratically. The net curvature is mainly positive but consistent with zero for the highest multiplicity class, although the fit error is large.

Figure 13 (right) shows the ratio $-k_Q/k_D = 16A_Q/A_D$ vs $\bar{\rho}_s$ for 200 GeV p - p collisions increasing linearly (solid line) from zero and passing through unity near the highest multiplicity class. As noted, for ratios significantly greater than 1 (significant negative net curvature) a SS ridge should appear within $|\eta_\Delta| > 1$. At higher collision energies and with additional p_t cuts the slope of the linear trend should increase, resulting in appearance of a significant SS ridge even for modest charge densities.

Figure 14 shows 2D angular correlations for $n = 1$ (left) and 6 (right) multiplicity classes. Fit-model elements for the soft component, BE + conversion electrons and constant offset have been subtracted from the data leaving the jet-related and NJ quadrupole components (see Fig. 4 for fit details). In the region $|\eta_\Delta| > 1$ that excludes the SS 2D peak we observe that near $\phi_\Delta = 0$ (SS) the cur-

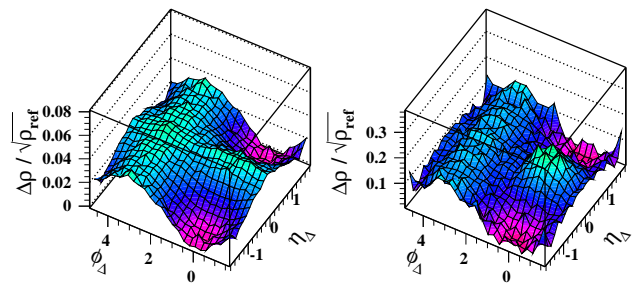


FIG. 14: 2D angular correlations for $n = 1$ (left) and 6 (right) multiplicity classes from 200 GeV p - p collisions. Fitted model elements for soft component, BE + conversion electrons and constant offset have been subtracted from the data leaving jet-related and NJ quadrupole data components.

vature varies from large and positive (left) to consistent with zero (right). Near $\phi_\Delta = \pi$ (AS) the negative curvature *approximately doubles*. The second variation is as much a part of the “ridge” phenomenon as the first, but is typically not acknowledged [11, 25].

Alteration of the SS 2D peak is also notable. Visually the peak appears to narrow dramatically on ϕ_Δ with increasing n_{ch} . However, 2D model fits reveal that the fitted peak width decreases only slightly. The *apparent* narrowing is due to superposition of the NJ quadrupole component onto the 2D peak structure. The change from left to right panel is dominated by the ten-fold increase of curvature ratio $|k_Q/k_D|$, as indicated in Fig. 13 (right).

B. RHIC vs LHC correlation structure

In Ref. [11] the systematics of 2D angular correlations derived from 62 and 200 GeV Au-Au collisions were extrapolated first to peripheral N - N collisions (as a proxy for NSD p - p collisions) and then to 7 TeV for comparisons with CMS p - p data. The question posed: Are SS 2D peak, AS dipole and NJ quadrupole systematics at and below 200 GeV consistent with those at 7 TeV and especially with the emergence of a SS “ridge” structure for certain conditions imposed at that energy? As to p - p estimates, at 200 GeV the NSD p - p values of A_{2D} and A_D from the present study are numerically consistent with the Au-Au extrapolation to N - N collisions. The value of A_Q for 200 GeV p - p collisions was overestimated by a factor 2 by addition of a conjectured quadrupole contribution from the AS 1D peak modeled as a 1D Gaussian. According to the present study the AS peak for p - p collisions is actually well described by a single dipole element.

It was demonstrated that dijet production at 7 TeV is consistent with extrapolation from 200 GeV using factor $R(\sqrt{s}) = 2.3$ (derived from comparison of 62 and 200 GeV data) interpreted to describe the increase of participant low- x gluons with increasing collision energy. That factor applies to the *per-particle* SS 2D peak amplitude A_{2D} (intrajet correlations), whereas increase of

TABLE II: p - p correlation systematics. Entries represent systematics inferred from RHIC data at 0.2 TeV and extrapolations inferred by modeling CMS angular correlation histograms at 7 TeV from Ref. [25]. The left columns indicate collision energy and cut conditions, including minimum-bias (MB) data. The A_X represent parameters from the present per-particle analysis with an intensive correlation measure. The corresponding CMS measures are defined by $R_x = (2\pi \times 4.8)A_X \approx 30A_X$ [11].

\sqrt{s} (TeV)	Condition	$100A_Q$	A_D	A_{2D}	$16A_Q/A_D$
0.2	NSD	0.05 ± 0.02	0.05 ± 0.002	0.06 ± 0.002	0.16 ± 0.07
0.2	$n = 6$	0.84 ± 0.15	0.18 ± 0.012	0.26 ± 0.05	0.75 ± 0.17
7	MB	0.12 ± 0.04	0.07 ± 0.01	0.14 ± 0.01	0.27 ± 0.12
7	$N_{trk} > 110$	1.8 ± 0.6	0.28 ± 0.04	0.56 ± 0.04	1.03 ± 0.3
7	p_t, n_{ch} cuts	1.2 ± 0.4	0.14 ± 0.02	0.28 ± 0.02	1.37 ± 0.4

AS dipole amplitude A_D (jet-jet correlations) is considerably less (consistent with no amplitude increase from 62 to 200 GeV [20]). NJ quadrupole measurements at RHIC suggest that A_Q also increases by factor 2.3.

As to multiplicity trends for p - p collisions, in the present study the corrected charge density for multiplicity class $n = 6$ is $\bar{\rho}_0 = 13.7$, 5.5 times the MB value 2.5, whereas at 7 TeV the CMS $N_{trk} > 110$ multiplicity class corresponds to corrected $\bar{\rho}_0 = 136/4.8 = 28$, 4.8 times the MB value 5.8. In this study the $n = 6$ class corresponds to measured four-fold increase of A_D and A_{2D} and fifteen-fold increase of A_Q over their MB values.

As to responses to p_t cuts we note that about half of all MB jet fragments appear below the mode of the 200 GeV spectrum hard component at 1 GeV/c [4, 19]. In contrast, the mode of $v_2(p_t)$ on p_t is close to 3 GeV/c [36]. The CMS cut $p_t \in [1, 3]$ GeV/c is effectively a lower limit at 1 GeV/c, since the hadron spectrum falls rapidly with p_t . We thus expect that a p_t lower limit imposed at 1 GeV/c should reduce the AS dipole substantially more than the NJ quadrupole. We have reduced A_D by factor 1/2 and A_Q by factor 2/3 to estimate the effect of p_t cuts.

Table II summarizes the various estimates. The first two rows report results from the present study and the curvature ratios shown in Fig. 13. As noted in the text the 7 TeV MB values are obtained by multiplying A_{2D} and A_Q by 2.3 and A_D by 1.4. The values for $N_{trk} > 110$ are obtained with factors 4 and 15 applied as for the 200 GeV values for $n = 6$ (ignoring the small difference in ratios to MB multiplicities between RHIC and LHC energies). The effect of the p_t cut is estimated by factors 1/2 and 2/3 as noted above.

Results from the present study describe the reported CMS 7 TeV 2D angular correlations quantitatively and are generally consistent with Ref. [11] but also provide insight into the physical origins of the reported SS ‘‘ridge.’’ The large collision-energy increase combined with imposed p_t and multiplicity cuts increases the p - p NJ quadrupole amplitude eight-fold relative to the AS 1D jet peak, changing the SS curvature sign and producing an apparent SS ridge. In effect, the SS azimuth curvature functions as a comparator, switching from valley to ridge as one amplitude increases relative to another. A quantitative curvature change is transformed to a qualitative shape change (mis)interpreted as emergence of a novel phenomenon at a higher energy.

XII. DISCUSSION

Several open issues for high-energy p - p collisions were summarized in Sec. II: (a) the role of p - p collision centrality, (b) the definition and nature of the p - p underlying event or UE, (c) the systematics of MB dijet production and (d) confirmed existence and characteristics of a NJ quadrupole component in p - p angular correlations. We return to those points in light of results from this study.

A. Dijets vs NJ quadrupole vs flows

The measured hard components of y_t spectra, η densities and 2D angular correlations presented in this study complete a unified experimental and theoretical picture of MB dijet production (no p_t cuts) established previously for Au-Au collisions [18–20]. There were no previous measurement of a NJ quadrupole component for p - p collisions. The combined dijet and quadrupole results from the present study convey important implications for claims of p - p collectivity (flows), p - p centrality, UE studies and the mechanism of the CMS ridge.

The term ‘‘collective’’ or ‘‘collectivity’’ (e.g. as recently applied to small collision systems at the LHC) is ambiguous, since jet formation is a form of ‘‘collectivity’’ as is the NJ quadrupole whatever its production mechanism. Introducing the term ‘‘collectivity’’ as synonymous with ‘‘flow’’ may produce confusion. There are certainly collective aspects of p - p collisions although it is unlikely that hydrodynamic flow (in the sense of fluid motion resulting from particle rescattering) plays a role. Dijet production and the NJ quadrupole amplitude follow characteristic trends on $\bar{\rho}_s$ precisely over a large range of amplitudes (100-fold for dijets, 1000-fold for quadrupole as correlated-pair numbers) while the underlying particle (participant-gluon) density varies 10-fold. How can a small collision system with extremely low particle density support a hydrodynamic phenomenon that conspires to follow the same trends over such a large density interval?

B. p-p centrality and IS geometry

The notion of centrality (impact parameter) for p - p collisions is ambiguous in principle. Concerning p - p cen-

trality several questions arise: What does “IS geometry” mean for p - p collisions? Is an impact parameter relevant? How are total n_{ch} , triggered dijets, transverse low- x parton (gluon) density and p - p centrality correlated? How do those factors relate to measured ensemble-mean PDFs, *event-wise* participant-parton distributions on x and initial momentum transfer? There are certainly large event-wise fluctuations in soft-hadron and dijet production, but whether those correspond to fluctuations of p - p IS transverse geometry or some other collision aspect is in question. The need for comprehensive study of the n_{ch} dependence of p - p angular correlations in relation to p - p centrality was one motivation for the present study.

Results from this study support two arguments against a major role for a p - p centrality concept: (a) p - p dijet production scales as $N_{bin} \propto N_{part}^2 \sim \bar{\rho}_s^2$ but the eikonal approximation implies binary-collision scaling as $N_{bin}(b) \propto N_{part}^{4/3}(b)$ (as for A - A collisions). The observed dijet trend is consistent with encounters between all possible participant-gluon pairs in each collision, not a smaller subset determined by an impact parameter. (b) The NJ quadrupole amplitude scales as $N_{part}N_{bin} \sim \bar{\rho}_s^3$ over a large n_{ch} range consistent with *part* of the $N_{part}N_{bin}\epsilon_{opt}^2$ trend observed for A - A collisions, but there is no significant reduction with a decreasing p - p eccentricity. The combined trends suggest that p - p IS geometry is not a determining factor for either phenomenon. Instead, the event-wise depth of penetration on momentum fraction x of the projectile wave function may be the main source of variation for soft, hard and quadrupole components.

C. Implications for UE studies

As noted in Sec. II UE studies rely on several assumptions: (a) Concentration of low- x gluons at small radius in the proton (inferred from DIS data) provides a correlation among p - p centrality, soft hadron production and dijet production, (b) the conventionally-defined TR on azimuth includes no contribution from a triggered dijet and (c) multiple-parton interactions (MPI) may occur in jet-triggered p - p collisions. The integrated TR yield denoted by N_{\perp} is observed to increase with increasing jet-trigger p_t condition and is interpreted to represent a soft background increasing with p - p centrality.

Reference [12] addressed part of that narrative with simulations based on the TCM for hadron production from p - p collisions. It concluded that most dijets (what would result from an applied trigger at lower p_t) emerge from *low*-multiplicity collisions. Spectrum studies already indicated that higher-multiplicity collisions do produce dijets at higher rates but are few in number and so contribute only a small fraction of the p_t -triggered event population. A p_t condition cannot significantly alter the soft component or p - p collision centrality (if relevant).

The present study adds the following new information: (a) 2D angular correlations confirm a strong contribution from MB dijets *within the TR*. (b) The dijet production

trend $\propto \bar{\rho}_s^2$ suggests that the eikonal approximation is invalid and that centrality is not a useful concept for p - p collisions. (c) Monotonic increase of the NJ quadrupole $\propto \bar{\rho}_s^3$ over a large n_{ch} range also suggests that p - p centrality, as manifested in a varying IS eccentricity, is not a useful concept. Those factors confirm the conclusions of Ref. [12] and lead to the following scenario for N_{\perp} variation with a p_t trigger: As the trigger condition is increased from zero the integrated spectrum soft component increases N_{\perp} from zero to a plateau on $p_{t,trig}$. The hard-component (jet) contribution to N_{\perp} is similarly integrated up to a plateau. N_{\perp} thus has both soft and hard components exhibiting plateau structures slightly displaced from one another on $p_{t,trig}$. Almost all events satisfying an increased trigger condition contain a dijet (are hard events) but remain characteristic of a MB population with smaller soft multiplicity, not the expected more-central population with larger soft multiplicity.

Given the observed n_{ch} -dependent structure of p - p 2D angular correlations we arrive at three conclusions: (a) All dijets include a large-angle base that strongly overlaps the TR. That base dominates minimum-bias jets but may persist within all higher-energy (e.g. p_t -triggered) dijets. (b) The region with a minimal dijet contribution that might suffice for UE studies is defined by $|\eta_{\Delta}| > 1$ and $\phi_{\Delta} \approx 0$ (see Fig. 14). An immediate example of novel UE structure that might be discovered there is provided by the CMS “ridge,” a manifestation of the NJ quadrupole that was not expected in p - p collisions. (c) The likelihood of multiple dijet production in p_t -triggered events (which retain a low soft multiplicity as noted) is small whereas the likelihood of multiple dijets in high-multiplicity events approaches unity. The usual interpretation of N_{\perp} trends in terms of MPI may be misleading.

D. TCM confirmation and self-consistency

Arguments against the TCM have been presented since commencement of RHIC operation. It has been noted that the HIJING Monte Carlo [17] (based on PYTHIA [15]) fails to describe RHIC and LHC A - A data. That failure has been expressed as “too slow increase” of hadron production with centrality and energy [51, 52]. HIJING is assumed to represent the TCM and its failure is then confused with failure of the TCM itself, of which HIJING is only a specific theory implementation. The problems with HIJING are traceable to the eikonal-model assumption included in default PYTHIA [20]. Such arguments typically rely on data from a centrality range covering only the more-central 40-50% of the A - A cross section [51, 53]. The critical centrality region extending from p - p or N - N collisions to the *sharp transition* in jet formation [20] is not considered. Alternative models that seem to describe the more-central data are actually falsified by more-peripheral data [50]. An alternative argument is based on assuming that TCM agreement with data is accidental, that a *constituent-quark* model (soft

only, excluding jets) is more fundamental and describes data as well [54], but that argument is questionable [23].

The TCM invoked in this study is based on previous analysis of p_t spectrum n_{ch} and centrality dependence [4, 18–20, 26], p_t fluctuations and correlations [27, 33, 34], transverse-rapidity $y_t \times y_t$ correlations [5, 35] and minimum-bias 2D number angular correlations [5, 6, 20]. In each case model elements were determined quantitatively by systematic analysis without regard to physical mechanisms. Only after the TCM was so established were connections with theory and physical interpretations introduced. In the present study we extend the TCM to describe the n_{ch} dependence of 200 GeV p - p η densities and 2D angular correlations. In the latter we observe for the first time a significant NJ quadrupole component and its n_{ch} dependence as a novel nonjet phenomenon within the UE. We find that the extended TCM remains fully self-consistent and provides accurate and efficient representation of a large body of data.

XIII. SUMMARY

We report measurements of the charge-multiplicity dependence of single-particle (SP) densities on transverse rapidity y_t (as y_t spectra) and pseudorapidity η and 2D angular correlations on (η, ϕ) from 200 GeV p - p collisions. The SP densities are described accurately by a two-component (soft + hard) model (TCM) of hadron production. The inferred y_t -spectrum TCM is consistent with a previous study. The result for η densities newly reveals the distribution on η of minimum-bias (MB) jet fragments. 2D angular correlations are fitted with a multi-element fit model previously applied to data from 62 and 200 GeV Au-Au collisions. Fit residuals are consistent with statistical uncertainties in all cases.

Trends for several 2D correlation model parameters are simply expressed in terms of TCM soft-component multiplicity n_s or mean density $\bar{\rho}_s \equiv n_s/\Delta\eta$ ($\Delta\eta$ is a detector acceptance). Correlated-pair numbers for soft component (projectile dissociation) scale $\propto \bar{\rho}_s$, for hard component (dijet production) scale $\propto \bar{\rho}_s^2$ and for nonjet (NJ) quadrupole scale $\propto \bar{\rho}_s^3$. The NJ quadrupole amplitude is quite significant for higher-multiplicity p - p collisions.

The dijet production trend is inconsistent with an

eikonal approximation for p - p collisions (which would require dijets $\propto \bar{\rho}_s^{4/3}$), and the monotonically-increasing NJ quadrupole trend is inconsistent with an initial-state eccentricity determined by p - p impact parameter. The two trends combined suggest that centrality is not a useful concept for p - p collisions. Fluctuations may instead depend on the event-wise depth of penetration on momentum fraction x of the projectile wave functions and in turn on the number of participant low- x partons.

2D angular-correlation data are in conflict with assumptions relating to the p - p underlying event (UE, the complement to a triggered dijet). The azimuth transverse region (TR) bracketing $\pi/2$ is assumed to contain no contribution from a triggered dijet, but minimum-bias dijets are observed to make a strong contribution there. The region with minimal jet contribution is defined by $|\eta_\Delta| > 1$ near the azimuth origin that excludes the same-side 2D jet peak and most of the away-side 1D jet peak.

The presence of a significant NJ quadrupole component and its multiplicity trend have several implications: (a) initial-state transverse geometry does not appear to be a useful concept for p - p collisions as noted above, (b) the appearance of a NJ quadrupole component in a small system with negligible particle density contradicts the concept of a hydro phenomenon based on particle rescattering and large energy/particle density gradients and (c) the same-side “ridge” observed in p - p collisions at the large hadron collider (LHC), interpreted by some to suggest “collectivity” (flows) in small systems, results from an interplay of the jet-related away-side 1D peak and the NJ quadrupole that together determine the curvature on azimuth near the origin. When that curvature transitions from positive to negative (depending on collision energy and other applied cuts) a same-side “ridge” appears.

In a hydro narrative the NJ quadrupole component interpreted as elliptic flow should represent azimuth modulation of radial flow detected as a modification of SP y_t spectra. But no corresponding modification is observed in p - p y_t spectra despite precise differential analysis.

This material is based upon work supported by the U.S. Department of Energy Office of Science, Office of Nuclear Physics under Award Number DE-FG02-97ER41020.

-
- [1] L. Frankfurt, M. Strikman and C. Weiss, Phys. Rev. D **83**, 054012 (2011).
 - [2] T. Affolder *et al.* (CDF Collaboration), Phys. Rev. D **65**, 092002 (2002).
 - [3] V. Khachatryan *et al.* (CMS Collaboration), Eur. Phys. J. C **70**, 555 (2010).
 - [4] J. Adams *et al.* (STAR Collaboration), Phys. Rev. D **74**, 032006 (2006).
 - [5] R. J. Porter and T. A. Trainor (STAR Collaboration), J. Phys. Conf. Ser. **27**, 98 (2005).
 - [6] R. J. Porter and T. A. Trainor (STAR Collaboration), PoS C **FRNC2006**, 004 (2006).
 - [7] T. A. Trainor, D. T. Kettler, D. J. Prindle and R. L. Ray, J. Phys. G **42**, no. 2, 025102 (2015).
 - [8] D. T. Kettler, D. J. Prindle and T. A. Trainor, Phys. Rev. C **91**, 064910 (2015).
 - [9] D. T. Kettler (STAR collaboration), Eur. Phys. J. C **62**, 175 (2009).
 - [10] D. Kettler (STAR Collaboration), J. Phys. Conf. Ser. **270**, 012058 (2011).

- [11] T. A. Trainor and D. T. Kettler, Phys. Rev. C **84**, 024910 (2011).
- [12] T. A. Trainor, Phys. Rev. D **87**, no. 5, 054005 (2013).
- [13] T. A. Trainor, Mod. Phys. Lett. A **23**, 569 (2008).
- [14] P. Bartalini *et al.*, arXiv:1111.0469 [hep-ph].
- [15] T. Sjöstrand and M. van Zijl, Phys. Rev. D **36**, 2019 (1987).
- [16] R. Field, Acta Phys. Polon. B **42**, 2631 (2011).
- [17] X.-N. Wang, Phys. Rev. D **46**, R1900 (1992); X.-N. Wang and M. Gyulassy, Phys. Rev. D **44**, 3501 (1991).
- [18] T. A. Trainor, Int. J. Mod. Phys. E **17**, 1499 (2008).
- [19] T. A. Trainor, Phys. Rev. C **80**, 044901 (2009).
- [20] G. Agakishiev, *et al.* (STAR Collaboration), Phys. Rev. C **86**, 064902 (2012).
- [21] T. A. Trainor and D. T. Kettler, Phys. Rev. C **83**, 034903 (2011).
- [22] S. Gavin, L. McLerran and G. Moschelli, Phys. Rev. C **79**, 051902 (2009).
- [23] T. A. Trainor, Phys. Rev. C **91**, no. 4, 044905 (2015).
- [24] B. Z. Kopeliovich, A. H. Rezaeian and I. Schmidt, Phys. Rev. D **78**, 114009 (2008).
- [25] CMS Collaboration, JHEP **1009**, 091 (2010).
- [26] T. A. Trainor, Phys. Rev. C **90**, no. 2, 024909 (2014).
- [27] T. A. Trainor, Phys. Rev. C **92**, no. 2, 024915 (2015).
- [28] J. Adams *et al.* (STAR Collaboration), Phys. Rev. C **73**, 064907 (2006).
- [29] J. Adams *et al.* (STAR Collaboration), Phys. Lett. B **634**, 347 (2006).
- [30] T. A. Trainor, R. J. Porter and D. J. Prindle, J. Phys. G **31**, 809 (2005).
- [31] R. J. Porter and T. A. Trainor (STAR Collaboration), Acta Phys. Polon. B **36**, 353 (2005).
- [32] B. S. Everitt and A. Skrondal, "The Cambridge Dictionary of Statistics," 4th Ed., (Cambridge University Press, Cambridge, 2010), p. 107.
- [33] J. Adams *et al.* (STAR Collaboration), J. Phys. G **32**, L37 (2006).
- [34] J. Adams *et al.* (STAR Collaboration), J. Phys. G **33**, 451 (2007).
- [35] E. W. Oldag (STAR Collaboration), J. Phys. Conf. Ser. **446**, 012023 (2013).
- [36] J. Adams *et al.* (STAR Collaboration), Phys. Rev. C **72**, 014904 (2005).
- [37] P. Huovinen and P. V. Ruuskanen, Ann. Rev. Nucl. Part. Sci. **56**, 163 (2006).
- [38] T. A. Trainor, Phys. Rev. C **78**, 064908 (2008).
- [39] D. Acosta *et al.* (CDF Collaboration), Phys. Rev. D **68**, 012003 (2003).
- [40] C. Albajar *et al.* (UA1 Collaboration), Nucl. Phys. B **309**, 405 (1988).
- [41] T. A. Trainor, Phys. Rev. D **89**, no. 9, 094011 (2014).
- [42] T. A. Trainor, J. Phys. G **37**, 085004 (2010).
- [43] T. A. Trainor, Phys. Rev. C **81**, 014905 (2010).
- [44] Ya. I. Azimov, Yu. L. Dokshitzer, V. A. Khoze, S. I. Troyan, Z. Phys. C **27**, 65 (1985), Z. Phys. C **31**, 213 (1986).
- [45] G. Wolschin, Phys. Rev. C **91**, 014905 (2015).
- [46] T. A. Trainor, J. Phys. G **40**, 055104 (2013).
- [47] T. A. Trainor, D. J. Prindle and R. L. Ray, Phys. Rev. C **86**, 064905 (2012).
- [48] M. B. De Kock, H. C. Eggers and T. A. Trainor, Phys. Rev. C **92**, no. 3, 034908 (2015).
- [49] B. I. Abelev *et al.* (STAR Collaboration), Phys. Rev. C **80**, 064912 (2009).
- [50] T. A. Trainor, J. Phys. G **39**, 095102 (2012).
- [51] M. Gyulassy and L. McLerran, Nucl. Phys. A **750**, 30 (2005).
- [52] B. B. Back *et al.* (PHOBOS Collaboration), Phys. Lett. B **578**, 297 (2004).
- [53] D. Kharzeev and E. Levin, Phys. Lett. B **523**, 79 (2001).
- [54] S. S. Adler *et al.* (PHENIX Collaboration), Phys. Rev. C **89**, no. 4, 044905 (2014).